Expected Collision Rates for Tracked Satellites

Doyle T. Hall*
Omitron Incorporated, Colorado Springs, Colorado 80903

https://doi.org/10.2514/1.A34919

This analysis estimates collision risks between tracked satellites based on the statistically expected collision rate $\dot{N}_c$ and number of collisions N_c, which are closely related to the collision probability P_c. For isolated encounters, N_c equals P_c. For multi-encounter interactions, N_c can exceed P_c and is significantly easier to approximate semi-analytically. Estimating N_c requires integrating the collision rate over time throughout an interaction, with each required $\dot{N}_c$ value calculated as a statistical expectation value based on the uncertainty distributions of initial orbital states. The uncertainty distributions are estimated from orbit determination analyses of satellite trajectory measurements. The formulation accounts for the nonlinear orbital motion of the satellites, and derives N_c and $\dot{N}_c$ expressions for Monte Carlo simulations as well as semi-analytical approximations for single- and multi-encounter interactions.

Nomenclature

$\bar{\boldsymbol{A}}$ = marginalized relative position covariance estimated at $\bar{\boldsymbol{X}}$
$\tilde{\boldsymbol{A}}$ = marginalized relative position covariance estimated at $\tilde{\boldsymbol{X}}$; see Eq. (47)
$\bar{\boldsymbol{A}}_j$ = marginalized position covariance estimated at the position–velocity vector $\bar{\boldsymbol{X}}_j$ for satellite j
$\tilde{\boldsymbol{A}}_j$ = marginalized position covariance estimated at $\tilde{\boldsymbol{X}}_j$; see Eq. (44)
$\boldsymbol{a}$ = inertial position vector used when examining the product of two position probability density functions
a_f = second equinoctial orbital element
a_g = third equinoctial orbital element
$\tilde{\boldsymbol{\alpha}}_j(t)$ = two-body equinoctial-to-Cartesian 6×6 transformation matrix of partial derivatives evaluated at the position–velocity vector $\tilde{\boldsymbol{X}}_j(t)$
$\bar{\boldsymbol{B}}$ = relative velocity–position cross covariance estimated at $\bar{\boldsymbol{X}}$
$\tilde{\boldsymbol{B}}$ = relative velocity–position cross-covariance estimated at $\tilde{\boldsymbol{X}}$; see Eq. (47)
$\bar{\boldsymbol{B}}_j$ = velocity–position cross-covariance estimated at the position–velocity vector $\bar{\boldsymbol{X}}_j$ for satellite j
$\tilde{\boldsymbol{B}}_j$ = velocity–position cross-covariance estimated at $\tilde{\boldsymbol{X}}_j$; see Eq. (44)
b = ballistic-coefficient auxiliary orbital state variable
$\bar{\boldsymbol{C}}$ = marginalized velocity covariance estimated at $\bar{\boldsymbol{X}}$
$\tilde{\boldsymbol{C}}$ = marginalized velocity covariance estimated at $\tilde{\boldsymbol{X}}$; see Eq. (47)
$\tilde{\boldsymbol{C}}'$ = conditional relative velocity covariance; see Eqs. (49) and (50)
$\bar{\boldsymbol{C}}_j$ = marginalized velocity covariance estimated at the position–velocity vector $\bar{\boldsymbol{X}}_j$ for satellite j
$\tilde{\boldsymbol{C}}_j$ = marginalized velocity covariance estimated at $\tilde{\boldsymbol{X}}_j$; see Eq. (44)
c = solar radiation pressure parameter auxiliary orbital state variable
$\mathcal{D}$ = ensemble of model/environmental data sets required for special-perturbation orbital state propagation
$d\hat{\boldsymbol{r}}$ = differential area on the surface of the unit sphere ($\oint \mathrm{d}\hat{\boldsymbol{r}}$ represents an integral over the entire unit sphere)
$\mathbb{E}$ = statistical expected value operator for interactions involving two satellites
E = number of egresses that occur during $\tau_a \le t < \tau_b$
$\boldsymbol{E}_j$ = equinoctial orbital element vector for satellite j
$\boldsymbol{E}_j^k$ = equinoctial orbital element vector for satellite j at the time of closest approach T^k; sometimes used with the index k suppressed for brevity
$\bar{\boldsymbol{E}}_j^k$ = equinoctial element vector for satellite j at T^k propagated from the mean orbital state; sometimes used with the index k suppressed for brevity
$\tilde{\boldsymbol{E}}_j^k$ = equinoctial element vector used as the center point of a Taylor series; see Eqs. (39) and (41); sometimes used with the index k suppressed for brevity
$\boldsymbol{E}_{j,0}$ = equinoctial orbital element vector for satellite j at the initial time $t_{j,0}$
E^m = number of egresses that occur during $\tau_a \le t < \tau_b$ in the mth Monte Carlo trial
e = index counting egress events, in which two circumscribing spheres cease to overlap
F_o = function that indicates the overlap status between two spheres
$H(\tilde{\nu})$ = factor of the relative velocity integral $\nu(\hat{\boldsymbol{r}}, \breve{\boldsymbol{X}}, \tilde{\boldsymbol{P}})$; see Eq. (52)
I = number of ingresses (or collisions) that occur during the time interval $\tau_a \le t < \tau_b$
I^m = number of ingresses (or collisions) that occur during $\tau_a \le t < \tau_b$ in the mth Monte Carlo trial
i = index counting ingress events, in which two circumscribing spheres begin to overlap
j = satellite index, with 1 denoting the primary and 2 the secondary
K = number of encounter segments that span the risk-assessment interval $\tau_a \le t < \tau_b$
k = encounter segment index
M = total number of sampling trials performed in a Monte Carlo simulation
m = sampling trial index in a Monte Carlo simulation
$\mathcal{N}$ = multivariate normal function; see Eq. (11)
N_c = statistically expected number of collisions
$\dot{N}_c$ = statistically expected collision rate (i.e., the time derivative of N_c)
$\dot{N}_c^D$ = deterministic collision rate, which represents the nonnegative part of $\dot{N}_o^D$
N_c^k = expected collision number within the kth encounter segment
$\dot{N}_c^k$ = expected collision rate within the kth encounter segment

Received 3 August 2020; revision received 18 September 2020; accepted for publication 22 October 2020; published online Open Access 29 January 2021.

*Senior Conjunction Assessment Research Scientist, 555 E. Pikes Peak Ave, #205.

N_c^{MC} = expected collision number for a Monte Carlo simulation
$\dot{N}_c^{\mathrm{MC}}$ = expected collision rate for a Monte Carlo simulation
$\dot{N}_{\mathrm{fc}}^D$ = deterministic first-contact collision rate, which only includes the earliest ingress event
N_o^D = deterministic overlap status (or number) for a pair of satellites
$\dot{N}_o^D$ = time derivative of N_o^D (i.e., the rate of change of the deterministic overlap status)
N_q = number of elements in a vector $\boldsymbol{q}$ of auxiliary orbital state variables
N_S = number of elements in an orbital state vector
n = mean motion (i.e., the first equinoctial orbital element)
$\bar{\boldsymbol{P}}$ = relative position–velocity state covariance estimated at the relative position–velocity state $\bar{\boldsymbol{X}}$
$\tilde{\boldsymbol{P}}$ = relative position–velocity state covariance estimated at the relative state $\breve{\boldsymbol{X}}$; see Eq. (47)
P_c = collision probability
$\dot{P}_c$ = collision probability rate (i.e., the time derivative of P_c)
$\bar{\boldsymbol{P}}_j$ = position–velocity state covariance estimated at the relative state $\bar{\boldsymbol{X}}_j$
$\tilde{\boldsymbol{P}}_j$ = position–velocity covariance for satellite j estimated at the expansion-center state $\tilde{\boldsymbol{X}}_j$; see Eq. (44)
$\bar{\mathbb{P}}_j$ = special-perturbation orbital state covariance matrix for satellite j
$\bar{\boldsymbol{\mathcal{P}}}_j^k$ = marginalized equinoctial covariance for satellite j at the time of closest approach T^k; see Eq. (33); sometimes used with the index k suppressed for brevity
$\bar{\mathbb{P}}_{j,0}$ = special-perturbation orbital state covariance matrix for satellite j at the initial time $t_{j,0}$
$\tilde{\boldsymbol{P}}_*$ = relative position–velocity state covariance estimated relative state $\tilde{\boldsymbol{X}}$, corrected for atmospheric density cross-correlation effects
$\mathbb{Q}_j(t, t_{j,0})$ = process noise matrix used to propagate the covariance for satellite j to time t from $t_{j,0}$
$\boldsymbol{q}_j$ = vector of auxiliary orbital state variables for satellite j
$\bar{\boldsymbol{q}}_j$ = vector of mean auxiliary orbital state variables for satellite j
R = combined circumscribing radii for the primary and secondary satellites, $R_1 + R_2$
R_j = radius of the sphere circumscribing satellite j
$\boldsymbol{r}$ = relative inertial position vector; see Eq. (4)
$\bar{\boldsymbol{r}}$ = relative position of the propagated mean orbital states of the two satellites
$\bar{r}$ = relative distance between the propagated mean orbital states of the two satellites
$\tilde{\boldsymbol{r}}$ = relative position component of the position–velocity vector $\tilde{\boldsymbol{X}}$
$\breve{\boldsymbol{r}}$ = relative position component of $\breve{\boldsymbol{X}}$, offset from position $\tilde{\boldsymbol{r}}$
$\hat{\boldsymbol{r}}$ = radial unit vector in a spherical coordinate system
$\boldsymbol{r}_j$ = inertial position vector for satellite j
$\bar{\boldsymbol{r}}_j$ = position of the propagated mean state for satellite j
$\tilde{\boldsymbol{r}}_j$ = position component of $\tilde{\boldsymbol{X}}_j$, used as the center of a Taylor series expansion
$\breve{\boldsymbol{r}}_j$ = position component of $\breve{\boldsymbol{X}}_j$, offset from the expansion-center position $\tilde{\boldsymbol{r}}_j$
$\boldsymbol{\mathcal{S}}$ = special-perturbation orbital state propagation function; see Eq. (12)
$\boldsymbol{S}_j$ = special-perturbation orbital state vector for satellite j
$\bar{\boldsymbol{S}}_j$ = special-perturbation orbital state vector propagated from the mean initial orbital state for satellite j
$\boldsymbol{S}_{j,0}$ = special-perturbation orbital state vector for satellite j at the initial time $t_{j,0}$
$\bar{\boldsymbol{S}}_{j,0}$ = mean special-perturbation orbital state vector for satellite j at the initial time $t_{j,0}$
T = time of closest approach for a single encounter
T^k = time of closest approach of the kth encounter segment for a multi-encounter interaction
T_A^k = time of the relative-distance maximum bounding the beginning of segment k
T_a^k = beginning time for the interval that $\dot{N}_c^k(t)$ is appreciably large during segment k
T_B^k = time of the relative-distance maximum bounding the end of segment k
T_b^k = ending time for the interval that $\dot{N}_c^k(t)$ is appreciably large during segment k
t = time
t' = alternate variable indicating time, used for integrations that span $\tau_a \le t' < t$
$\mathfrak{t}_e$ = time of the eth egress that occurs during the risk-assessment interval $\tau_a \le t < \tau_b$
$\mathfrak{t}_e^m$ = eth egress time that occurs during $\tau_a \le t < \tau_b$ in the mth Monte Carlo trial
$\mathfrak{t}_i$ = time of the ith collision or ingress that occurs during the interval $\tau_a \le t < \tau_b$
$\mathfrak{t}_i^m$ = ith collision or ingress time that occurs during $\tau_a \le t < \tau_b$ in the mth Monte Carlo trial
$t_{j,0}$ = initial time for satellite j
$U(x)$ = unit-step function for scalar quantity X
$\boldsymbol{v}$ = relative inertial velocity vector; see Eq. (4)
$\bar{\boldsymbol{v}}$ = relative velocity of the propagated mean orbital states of the two satellites
$\tilde{\boldsymbol{v}}$ = velocity component of the relative position–velocity state $\tilde{\boldsymbol{X}}$
$\breve{\boldsymbol{v}}$ = velocity component of $\breve{\boldsymbol{X}}$, offset from the expansion-center velocity $\tilde{\boldsymbol{v}}$
$\tilde{\nu}$ = argument for the factor $H(\tilde{\boldsymbol{v}})$ of the relative velocity integral $\nu(\hat{\boldsymbol{r}}, \breve{\boldsymbol{X}}, \tilde{\boldsymbol{P}})$; see Eq. (52)
$\breve{\boldsymbol{v}}'$ = conditional relative velocity vector; see Eqs. (49) and (50)
$\boldsymbol{v}_j$ = inertial velocity vector for satellite j
$\bar{\boldsymbol{v}}_j$ = velocity of the propagated mean state for satellite j
$\tilde{\boldsymbol{v}}_j$ = velocity component of $\tilde{\boldsymbol{X}}_j$, used as the center of a Taylor series expansion
$\breve{\boldsymbol{v}}_j$ = velocity component of $\breve{\boldsymbol{X}}_j$, offset from the expansion-center velocity $\tilde{\boldsymbol{v}}_j$
$\nu(\hat{\boldsymbol{r}}, \breve{\boldsymbol{X}}, \tilde{\boldsymbol{P}})$ = relative velocity integral of the single-encounter collision rate; see Eqs. (51) and (52)
$\bar{\boldsymbol{\mathcal{W}}}_j^k$ = equinoctial/auxiliary variable cross covariance for satellite j at time of closest approach T^k; see Eq. (33)
$\boldsymbol{X}$ = relative inertial position–velocity state vector; see Eq. (4)
$\bar{\boldsymbol{X}}$ = relative position–velocity state vector propagated from the mean orbital states of the two satellites
$\tilde{\boldsymbol{X}}$ = difference of the two expansion-center vectors (i.e., $\tilde{\boldsymbol{X}} = \tilde{\boldsymbol{X}}_2 - \tilde{\boldsymbol{X}}_1$)
$\breve{\boldsymbol{X}}$ = relative position–velocity state vector offset from the vector $\tilde{\boldsymbol{X}}$
$\boldsymbol{X}_j$ = inertial position–velocity state vector for satellite j
$\bar{\boldsymbol{X}}_j$ = position–velocity state vector propagated from the mean orbital state of satellite j
$\tilde{\boldsymbol{X}}_j$ = position–velocity state vector used as the center point of a Taylor series expansion for satellite j
$\breve{\boldsymbol{X}}_j$ = relative position–velocity state vector offset from the expansion-center vector $\tilde{\boldsymbol{X}}_j$; see Eq. (44)
$\boldsymbol{X}_{\mathrm{SP}}$ = function that propagates special-perturbation states in time to produce relative position–velocity vectors; see Eq. (18)
$\boldsymbol{\mathcal{X}}_{\mathrm{SP}}$ = function that propagates a special-perturbation orbital state in time to produce a position–velocity vector; see Eq. (16)

$\boldsymbol{X}_{\mathrm{TB}}$ = function that propagates equinoctial states for two interacting satellites using two-body equations of motion to produce relative position–velocity vectors
$\boldsymbol{\mathcal{X}}_{\mathrm{TB}}$ = function that propagates an equinoctial orbital state using two-body equations of motion to produce a position–velocity vector; the inverse of $\mathcal{E}_{\mathrm{TB}}$; see Eqs. (34) and (35)
x = scalar quantity representing the argument of a delta function or a unit-step function
$\bar{\boldsymbol{\mathcal{Z}}}_j^k$ = marginalized auxiliary variable covariance for satellite j at time of closest approach T^k; see Eq. (33)
$\boldsymbol{\beta}(t, T)$ = two-body motion state transition matrix for equinoctial orbital states; see Eq. (40)
$\tilde{\boldsymbol{\Gamma}}_j$ = sensitivity vector for satellite j estimated at the expansion-center point; see Eq. (57)
$\delta(x)$ = Dirac delta function (i.e., the unit impulse function) for scalar quantity x
$\delta(\boldsymbol{x})$ = multidimensional delta function for vector $\boldsymbol{x}$, which equals the product $\prod_i \delta(x_i)$
$\mathcal{E}_{\mathrm{TB}}$ = function that propagates position–velocity vectors using two-body equations of motion to produce equinoctial orbital element vectors; the inverse of $\boldsymbol{\mathcal{X}}_{\mathrm{TB}}$; see Eqs. (34) and (35)
λ_M = mean longitude (i.e., the sixth equinoctial orbital element)
$\boldsymbol{\mu}'$ = mean state for the consolidated probability density function of $\boldsymbol{X}_1$; see Eq. (48)
$\boldsymbol{\mu}_p$ = peak-overlap location (i.e., the mode of the joint position vector probability density function); see Eq. (55)
$\rho_{j,0}$ = probability density function for the initial orbital state vector of satellite j
ρ_0 = joint probability density function for the initial orbital state vectors of the primary and secondary satellites
$\boldsymbol{\Sigma}'$ = covariance matrix for the consolidated probability density function of $\boldsymbol{X}_1$; see Eq. (48)
$\boldsymbol{\Sigma}_p$ = covariance matrix for the joint position vector probability density function; see Eq. (55)
σ = factor of the relative velocity integral $\nu(\hat{\boldsymbol{r}}, \check{\boldsymbol{X}}, \tilde{\boldsymbol{P}})$; see Eq. (52)
$\sigma_{j/g}$ = 1-sigma variation of the relative atmospheric density error for satellite j; see Eq. (57)
τ_a = beginning time of a user-specified collision risk-assessment time interval
τ_a^k = clipped beginning time for encounter segment k; see Eqs. (7) and (59)
τ_b = ending time of a user-specified collision risk-assessment time interval
τ_b^k = clipped ending time for encounter segment k; see Eqs. (7) and (59)
χ = fourth equinoctial orbital element
$\boldsymbol{\Psi}_j(t, t_{j,0})$ = state transition matrix used to propagate the covariance for satellite j to time t from time $t_{j,0}$
ψ = fifth equinoctial orbital element
$\tilde{\boldsymbol{\Psi}}_j$ = Jacobian matrix for satellite j that converts equinoctial state deviations at the time of closest approach T into position–velocity state deviations at time t; see Eqs. (39) and (40)
ϱ = joint probability density function for the equinoctial elements of the two satellites at a time of closest approach; see Eq. (36)
ϱ_j = probability density function for the equinoctial elements of satellite j at a time of closest approach

I. Introduction

THE NASA Conjunction Assessment Risk Analysis (CARA) team estimates collision probabilities for a specific set of high-value Earth-orbiting satellites [1] based on the latest available satellite tracking data and orbit determination (OD) solutions [2]. For each conjunction, CARA initially assesses collision risk using a set of semi-analytical P_c estimation methods [3,4], which are computationally efficient because they employ several simplifying assumptions, including linear trajectories. Unfortunately, such methods fail to provide accurate P_c estimates for some interactions, including multiple encounters between closely orbiting objects [4]. Although these can be addressed using Monte Carlo (MC) simulations [5–8], the computations required for high-fidelity MC-P_c estimates can be potentially prohibitive [8,9].

Like CARA, many other conjunction analysis organizations use P_c as a means to assess collision risk. This analysis formulates two alternate, but closely related, measures of collision risk: the statistically expected collision rate $\dot{N}_c$ and the associated expected number of collisions N_c. Together, these provide a means to quantify collision risks for single- or multi-encounter interactions, using both MC simulations and semi-analytical approximations.

II. Previous Work

Collision probabilities between tracked Earth-orbiting satellites have been discussed extensively during the past decades, resulting in MC estimation methods [5–8] and semi-analytical approximations (see Refs. [3,4,10–18]). Because manufactured satellites generally have irregular shapes, these methods usually estimate P_c for the spheres that circumscribe the objects [4,19].

A. "2-D P_c" Semi-Analytical Collision Probability Estimation

In 1992, Foster and Estes [3] introduced a method to estimate P_c for single encounters that employs three simplifying assumptions: the relative satellite motion can be approximated as linear during the conjunction; the uncertainties on the relative satellite positions can be approximated using a single, time-invariant covariance matrix; and the uncertainties on the satellite velocities can be neglected altogether. These assumptions allow P_c values to be approximated semi-analytically using two-dimensional (2-D) numerical integration [3]. In 2000, Akella and Alfriend [10] used these same assumptions to show that P_c can be expressed equivalently as an integral over time:

$$P_c = P_c(\tau_a, \tau_b) = \int_{\tau_a}^{\tau_b} \mathrm{d}t\ \dot{P}_c(t) \tag{1}$$

The integrand $\dot{P}_c(t)$ represents an estimated collision probability rate, expressed in Eq. (1) as a function of time, but that also depends on many other conjunction parameters. For a linear-motion encounter, the integration limits can be taken as $\tau_a = -\infty$ and $\tau_b = \infty$, and Akella and Alfriend [10] show that the infinitely bounded time integral can be performed analytically, yielding the same P_c expression originally derived by Foster and Estes [3]. High-fidelity MC-P_c simulations indicate that most, but not all, isolated conjunctions between tracked Earth-orbiting satellites can be approximated sufficiently accurately using these 2-D P_c methods [8,11].

B. "3-D P_c" Semi-Analytical Collision Probability Estimation

Some conjunctions must be addressed using a different approach because they do not satisfy all of the 2-D P_c assumptions [4–8]. Several authors have formulated semi-analytical approaches relaxing the 2-D P_c assumptions [4,12–17]. In 2012, Coppola [13] formulated a method for single encounters designed to account for nonlinear orbital motion and velocity uncertainties, resulting in an approximation for $\dot{P}_c(t)$ calculated using 2-D numerical integration over the surface of a unit sphere. When combined with a numerical 1-D time integration in the form of Eq. (1), this yields a 3-D P_c approximation. In 2015, Chan [16] contested the 3-D P_c formulation, arguing that a proper derivation must use a set of random variables associated with a time-invariant probability density function (PDF)—an approach explicitly adopted in this formulation.

In 2017, the CARA team implemented the 3-D P_c method in software [20], which uses as input the orbital states and covariances provided within a conjunction data message (CDM) [21]. Subsequent analysis indicated that, for some conjunctions, this approach produces P_c estimates that differ significantly from high-fidelity MC-P_c

values, even though all of the required 3-D P_c assumptions [13] are satisfied. The 2-D P_c method, however, accurately matches MC-P_c for most of these discrepant cases. In 2019, Shelton and Junkins [18] provided a key insight into why the 3-D P_c approximation fails for certain conjunctions. Their analysis indicates that accurate P_c approximations require that the PDFs of the two satellites be estimated accurately in the volume of space where they overlap the most. The original 3-D P_c formulation did not incorporate this concept, but this analysis does so explicitly.

C. Monte Carlo Simulation Collision Probability Estimation Methods

In 2011, Sabol et al. [6] described an MC estimation method for tracked Earth-orbiting satellites using high-fidelity special perturbations (SP) orbital propagation, which employs a complex and accurate dynamic model. That analysis describes two important aspects of high-fidelity MC-P_c estimation. First, using a Cartesian orbital state representation should be avoided because it inaccurately models uncertainties—an effect that can be mitigated by using an SP orbital state representation based on equinoctial orbital elements [23] supplemented by additional state parameters [6,24]. Second, state sampling and propagation in the MC simulations can be performed in two distinctly different ways [6]. States can be sampled from uncertainty PDFs estimated at the OD epoch times for both satellites, and then propagated forward throughout a collision risk-assessment interval that can span one or more encounters. Alternatively, states can be sampled from PDFs predicted for the time of closest approach (TCA) of a single conjunction, and propagated for short durations forward and backward from that time to assess the collision risk for that one encounter. In this analysis, these two approaches are referred to as "from epoch" and "from TCA," respectively, and both concepts will be extended to semi-analytical estimation methods.

III. Formulation for Expected Satellite Collision Rates and Derived Quantities

This section presents a summarized formulation for statistically expected collision rates and related quantities, with a methodology focused on interactions between tracked Earth-orbiting satellites. This section also presents top-level summary collision rate and probability expressions. The four following Secs. IV–VII present detailed derivations of these expressions.

A. Objectives

This analysis has the following five goals:

1) Formulate a methodology to derive expected satellite collision rates and probabilities, using a set of random variables to describe initial distributions of orbital states for the two interacting objects.

2) Apply the formulation to tracked Earth-orbiting satellites with OD solutions expressed in terms of SP states that are based on equinoctial orbital elements.

3) Derive collision rate and probability expressions for MC simulations that can be used for single encounters, as well as for interactions spanning multiple encounters.

4) Formulate semi-analytical approximations for collision rates expected for multi-encounter interactions, by dividing the interactions into independent single-encounter segments.

5) Formulate a semi-analytical method of approximating expected collision rates and probabilities for single encounters, and compare the results to MC simulations for a large set of archived events.

B. Methodology

The methodology used in this analysis differs from most previous studies in two fundamental ways. First, this formulation estimates collision risk by integrating rates over time, as in Eq. (1), but focuses primarily on deriving the expected number of collisions instead of the collision probability:

$$N_c(\tau_a, \tau_b) = \int_{\tau_a}^{\tau_b} \mathrm{d}t\ \dot{N}_c(t) \tag{2}$$

This is the number of collisions statistically expected to occur at some time during the risk-assessment interval $\tau_a \le t < \tau_b$, which, in this analysis, can represent either a short interval immediately bracketing a single close-approach encounter, or an extended interval spanning multiple encounters. The expected collision number is closely related to the collision probability. In fact, they are equal for single, temporally isolated encounters between well-tracked satellites: $N_c(\tau_a, \tau_b) = P_c(\tau_a, \tau_b)$. For intervals spanning multiple encounters, however, the expected collision number may exceed the collision probability: $N_c(\tau_a, \tau_b) \ge P_c(\tau_a, \tau_b)$. In the latter case, a key advantage of using N_c as a risk-assessment metric is that it can be calculated straightforwardly by dividing multi-encounter intervals into time segments, and integrating over each independently. Dividing multi-encounter interactions into independent time segments, however, cannot be done for P_c [4,16].

The second way this formulation differs from others is that it derives collision rates as statistical expectation values [25] using the following general expression, which is central to the methodology:

$$\begin{aligned}\dot{N}_c(t) &= \mathbb{E}[\dot{N}_c^D(\boldsymbol{X}(t))] \\ &= \int \mathrm{d}\boldsymbol{S}_{1,0} \int \mathrm{d}\boldsymbol{S}_{2,0} \rho_0(\boldsymbol{S}_{1,0}, \boldsymbol{S}_{2,0}) [\dot{N}_c^D(\boldsymbol{X}(t, \boldsymbol{S}_{1,0}, \boldsymbol{S}_{2,0}))]\end{aligned} \tag{3}$$

Sections IV and V describe the parts of this equation in detail, briefly summarized as follows:

1) The symbol $\mathbb{E}$ denotes the expected value operator for interactions involving two satellites.

2) The random variables $\boldsymbol{S}_{1,0}$ and $\boldsymbol{S}_{2,0}$ represent orbital state vectors for the primary and secondary satellites at the initial times $t_{1,0}$ and $t_{2,0}$, respectively. For from-epoch estimations, these initial times are the epochs of the OD solutions for the satellites, and $\boldsymbol{S}_{1,0}$ and $\boldsymbol{S}_{2,0}$ are full SP orbital state vectors (typically 8-D). For from-TCA estimations applicable to single encounters, both initial times equal the close approach time (i.e., $t_{1,0} = t_{2,0} = \mathrm{TCA}$), and the corresponding states are 6-D equinoctial orbital element vectors.

3) The two integrals indicate integrations over the entire domains of $\boldsymbol{S}_{1,0}$ and $\boldsymbol{S}_{2,0}$, respectively.

4) The PDF $\rho_0(\boldsymbol{S}_{1,0}, \boldsymbol{S}_{2,0})$ represents the joint uncertainty distribution for the initial orbital states of the two satellites. For statistically independent OD solutions, the joint PDF is equal to the product of the PDFs for the individual satellites: $\rho_0(\boldsymbol{S}_{1,0}, \boldsymbol{S}_{2,0}) = \rho_{1,0}(\boldsymbol{S}_{1,0})\rho_{2,0}(\boldsymbol{S}_{2,0})$.

5) The function $\dot{N}_c^D(\boldsymbol{X})$ represents the deterministic collision rate between the two satellites, expressed as a function of their relative position–velocity (PV) vector

$$\boldsymbol{X} = \boldsymbol{X}_2 - \boldsymbol{X}_1 = \begin{bmatrix} \boldsymbol{r} \\ \boldsymbol{v} \end{bmatrix} = \begin{bmatrix} \boldsymbol{r}_2 - \boldsymbol{r}_1 \\ \boldsymbol{v}_2 - \boldsymbol{v}_1 \end{bmatrix} \tag{4}$$

where $\boldsymbol{r}_j$ and $\boldsymbol{v}_j$ denote inertial-frame position and velocity vectors for satellite j.

6) The function $\boldsymbol{X}(t) = \boldsymbol{X}(t, \boldsymbol{S}_{1,0}, \boldsymbol{S}_{2,0})$ represents the relative PV vector predicted at time t, as propagated from the initial orbital states $\boldsymbol{S}_{1,0}$ and $\boldsymbol{S}_{2,0}$.

Section IV discusses orbital states, initial state distributions, and propagated state predictions in detail, focusing in particular on SP orbital states and associated OD solutions. Section V shows how the deterministic collision rate in the integrand of Eq. (3) can be expressed in a relatively simple form [22] that contains a Dirac delta function [32,33]:

$$\dot{N}_c^D(\boldsymbol{X}) = \delta(R^2 - |\boldsymbol{r}|^2)[-2(\boldsymbol{r} \cdot \boldsymbol{v})]_+ \tag{5}$$

where R denotes the combined circumscribing radii of the satellites; the delta function represents the derivative of the unit step function, $\delta(x) = dU(x)/dx$; and the $+$ subscript indicates the nonnegativity operator, $[x]_+ = \max(0, x)$. This collision rate would be expected in the idealized absence of any tracking uncertainties or OD modeling errors. Equation (5) also idealizes a collision as occurring whenever the spheres circumscribing the two satellites begin to overlap, and allows curved relative trajectories (such as orbits) the potential to create more than one such collision.

All expected collision rates and associated quantities formulated in this analysis are derived explicitly from Eqs. (2–5). Specifically, the next section presents expressions derived for use in MC simulations. Subsequent sections present semi-analytical approximations for $\dot{N}_c$ and N_c applicable to many single- and multi-encounter interactions between Earth-orbiting satellites.

C. Collision Rates and Probabilities for MC Simulations

Section VI shows how Eqs. (2–5) can be used to derive the expected collision rate and the expected collision number for MC simulations, which can be expressed as summations:

$$\dot{N}_c^{\mathrm{MC}}(t) = \frac{1}{M}\sum_{m=1}^{M}\left[\sum_{i=1}^{I^m}\delta(t-\mathfrak{t}_i^m)\right] \quad \text{and}$$
$$N_c^{\mathrm{MC}}(\tau_a,t) = \frac{1}{M}\sum_{m=1}^{M}\left[\sum_{i=1}^{I^m}U(t-\mathfrak{t}_i^m)\right] \tag{6}$$

where the superscript index $m = 1,\ldots,M$ spans the MC trials, and the set $\{\mathfrak{t}_i^m, i = 1,\ldots,I^m\}$ represents the ingress times during the mth trial (i.e., the times that the spheres circumscribing the two satellites begin to overlap as they approach one another). (Note: the summations in the square brackets in Eq. (6) are defined to be zero if $I^m = 0$.) The expressions for the MC collision probability are similar, but include only the first collision that occurs per trial [8] by retaining only the first summation term corresponding to $i = 1$ within the square brackets in Eq. (6) (see Sec. VI).

This MC formulation imposes no restrictions on the risk-assessment interval, $\tau_a \le t < \tau_b$, and can be used for either isolated encounters or multi-encounter interactions. In fact, the expressions derived in Sec. VI are equivalent to those implemented in the MC collision probability estimation software used by the CARA team [8], which has two primary modes: brute force Monte Carlo (BFMC) from-epoch estimations applicable to all interactions, but computationally demanding because of the required high-fidelity SP propagations, and two-body Monte Carlo (TBMC) from-TCA estimations, which are considerably more efficient, but restricted to temporally isolated encounters.

D. Semi-Analytical Collision Rates and Numbers for Single- and Multi-Encounter Interactions

Section VII shows how expected collision rates between two tracked satellites can be approximated semi-analytically, using an approach that addresses both single- and multi-encounter interactions. The first step entails dividing the risk-assessment interval into single-encounter time segments, which can be done using the predicted nominal separation distance between the two satellites, $\bar{r}(t)$. Figure 1 plots an illustrative example of $\bar{r}(t)$ for two commercial satellites in geosynchronous Earth orbit (GEO) [34], along with a notional 3 day risk-assessment interval $\tau_a \le t < \tau_b$ marked by vertical dashed lines. The minima on this curve (downward-pointing red triangles) each represent an approach between the satellites. The spans between successive maxima (upward-pointing blue triangles) define a sequence of "encounter segments" for the interaction. The example in Fig. 1 requires seven such encounter segments to span the entire risk-assessment interval, the first and last of which extend partially beyond the vertical dashed lines.

The expected number of collisions for the entire risk-assessment interval can be expressed as a sum of the contributions from the individual encounter segments:

$$N_c(\tau_a,\tau_b) = \sum_{k=1}^{K}[N_c^k] = \sum_{k=1}^{K}\left[\int_{\tau_b^k}^{\tau_a^k} \mathrm{d}t\ \dot{N}_c^k(t)\right] \tag{7}$$

where the superscript index $k = 1,\ldots,K$ denotes the sequential segments, $\dot{N}_c^k(t)$ indicates the collision rate approximated within segment k, and the integration bounds (τ_a^k, τ_b^k) typically only need to span a relatively short duration near each TCA (see Sec. VII). The

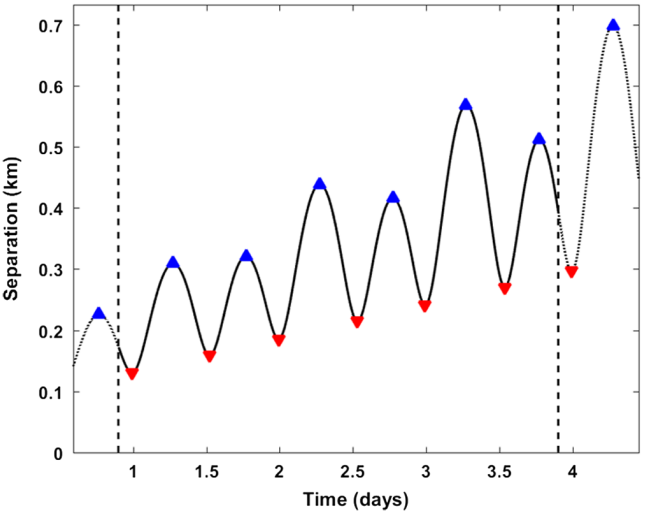

Fig. 1 Nominal separation distance between two closely orbiting GEO satellites.

1-D integrals in square brackets can be evaluated numerically [13,20].

The collision rate within each encounter segment in Eq. (7) can be approximated using 2-D numerical integration over the unit sphere, expressed as follows:

$$\dot{N}_c^k(t) \approx R^2 \oint \mathrm{d}\hat{\boldsymbol{r}}[\mathcal{N}(R\hat{\boldsymbol{r}},\check{\boldsymbol{r}}^k,\tilde{\boldsymbol{A}}^k)\nu(\hat{\boldsymbol{r}},\check{\boldsymbol{X}}^k,\tilde{\boldsymbol{P}}^k)] \tag{8}$$

Section VII provides a detailed derivation of Eq. (8) from Eq. (3), which is straightforward but lengthy, as well as a description of how to calculate the two integrand functions in the square brackets, and their time-dependent arguments $\check{\boldsymbol{r}}^k$, $\tilde{\boldsymbol{A}}^k$, $\check{\boldsymbol{X}}^k$, and $\tilde{\boldsymbol{P}}^k$. In summary, the formulation proceeds as follows:

1) Predict the mean SP state and associated covariance matrix for each satellite at the TCA of each encounter segment using high-fidelity propagation.

2) Approximate the orbital state PDF for each satellite at each TCA using the propagated mean equinoctial element vector, and the marginalized equinoctial state covariance matrix.

3) Neglect the effects of orbital perturbations during the effective duration of each encounter, allowing the trajectory for each satellite to be approximated using two-body equations of motion.

4) At each time during the encounter, approximate the nonlinear two-body motion for each satellite using a first-order Taylor series expansion, not centered on the mean states, but instead on states that coincide with the maximum overlap of the position PDFs of the two satellites. Determining each of these peak-overlap states requires an iterative calculation.

5) Using the converged peak-overlap states, evaluate and simplify the expected value integrals in Eq. (3), leading ultimately to the final expression given in Eq. (8).

Equations (7) and (8) provide the means to approximate the expected number of collisions N_c for single- or multi-encounter interactions. Each summed N_c^k term in Eq. (7) requires 3-D numerical integration, 1-D for the time integral and 2-D for the unit-sphere integral, and so this semi-analytical approximation method can be referred to as the "3-D N_c" method.

E. Semi-Analytical Collision Probability Approximation for Single-Encounter Interactions

For single, temporally isolated encounters, the expected collision rate equals the collision probability rate, both of which are given by Eq. (8). Notably, this expression has the same form as the probability rate derived in the original 3-D P_c formulation [13], but the arguments used in the integrand functions differ. Specifically, the original 3-D P_c integrand represents the approximation determined by using first-order series expansions centered on the mean orbital states,

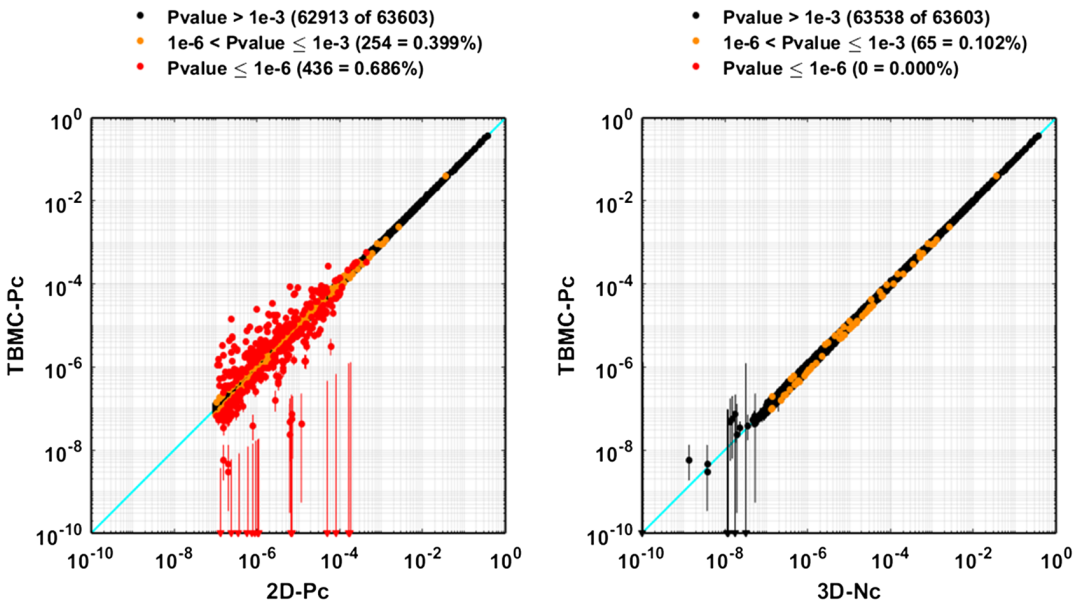

Fig. 2 Comparison of MC collision probabilities with the 2-D P_c method (left) and the 3-D N_c method introduced here (right), for a large set of CARA conjunctions.

which would be obtained by stopping the 3-D N_c algorithm after only one iteration. The first-order series used in the 3-D N_c method expands about states that coincide with the maximum overlap of the position PDFs of the two satellites, as determined by a fully converged iterative calculation (see Sec. VII).

Figure 2 shows a comparison of collision probabilities for 63,603 temporally isolated conjunctions extracted from the CARA database for events with 2-D $P_c > 10^{-7}$ archived between 1 May 2017 and 15 August 2019. The vertical axes on both panels plot MC estimates for the collision probability (specifically, from-TCA TBMC-P_c estimates), with error bars that show 95% confidence intervals estimated using the Clopper–Pearson method [35,36]. (Note that several of the conjunctions had zero hits registered in the MC simulations, which are represented in Fig. 2 using downward-pointing triangles and a single-sided error bar.) The horizontal axes plot the corresponding semi-analytical approximations: 2-D P_c on the left graph and 3-D N_c on the right graph. The colored points indicate the results of a binomial proportion statistical test that evaluates the agreement between the estimates [8]. Specifically, black points in Fig. 2 indicate P_c values that agree reasonably well, as they do not violate a null hypothesis that the two are equal at a p-value $\leq 10^{-3}$ significance level. However, those highlighted in yellow do violate the hypothesis at this significance level, and those in red at a more stringent level of p-value $\leq 10^{-6}$. Overall, the 2-D P_c comparison contains 254 yellow and 436 red points, which both significantly exceed the number of disagreements expected from purely statistical variations—even though together they represent a small fraction ($\sim$1%) of the original conjunctions. The 3-D N_c approximations clearly match the MC-P_c estimates better, producing only 65 yellow and zero red points. (Note that 13 3-D N_c estimates with values less than 10^{-10} are not plotted within the bounds of Fig. 2; these all also correspond to zero-hit MC simulations.) The comparison indicates that, for temporally isolated conjunctions, the 3-D N_c method produces more accurate estimates on average than the 2-D P_c method—although both are much more accurate on average than the CARA implementation [20] of the original 3-D P_c method, which is not plotted here.

F. Semi-Analytical Collision Probability Approximation for Multi-Encounter Interactions

Equations (7) and (8) provide a semi-analytical means to approximate the expected number of collisions for a multi-encounter interaction, $N_c(\tau_a, \tau_b)$. This analysis recommends using this quantity as a principal or auxiliary measure of collision risk in these situations, instead of the corresponding collision probability. (Again, for single, temporally isolated encounters, the two are identical.) However, the 3-D N_c method does provide lower and upper limiting P_c bounds for an unblended multi-encounter interaction: $\max_k[N_c^k] \leq P_c(\tau_a, \tau_b) \leq N_c(\tau_a, \tau_b)$. If a situation absolutely requires a probability estimate, and MC methods cannot be used due to scheduling or other constraints, then two options are available. The simpler, more conservative approach is to use the upper limit $N_c(\tau_a, \tau_b)$—or more accurately, $\min[1, N_c(\tau_a, \tau_b)]$—as an approximation for $P_c(\tau_a, \tau_b)$. A less conservative approach would be to use $P_c(\tau_a, \tau_b) \approx 1 - \prod_k (1 - N_c^k)$, which assumes that collision probabilities for the individual encounter segments are approximately statistically independent, which is unlikely the case for many interactions between Earth-orbiting satellites.

IV. Initial State Distributions and Orbital Propagation

This analysis formulates collision rates as statistical expectation values, based on initial orbital state distributions for the primary and secondary satellites. For tracked satellites, these distributions ideally represent PDFs that accurately quantify the uncertainties that arise from both imperfect trajectory measurements and deficiencies in the OD analysis process itself (e.g., inaccurate force models [2,9]). In broad terms, an OD solution for a satellite comprises an "OD epoch" time, plus a set of parameters used to express the uncertainty PDF of orbital states at that epoch.

This study focuses on high-fidelity OD solutions for Earth-orbiting satellites produced by the Astrodynamics Support Workstation (ASW) processing system, which employs SP orbital states along with a complex dynamic model and an advanced numerical integration scheme for orbital propagations [26,27]. Specifically, ASW incorporates the following components: a high-order expansion for the gravitational field of Earth, lunar/solar gravitation, solar radiation pressure (with Earth shadow), and atmospheric drag calculated using the latest version of the Jacchia–Bowman atmospheric density model [28] and the associated dynamic calibration atmosphere for the high accuracy satellite drag model [29].

A. Initial Orbital States and Uncertainty Distributions

Let $t_{1,0}$ and $t_{2,0}$ denote the OD epoch times for the primary and secondary satellites, respectively. The SP orbital states at these epochs can be expressed as vectors with two vector subcomponents:

$$\boldsymbol{S}_{j,0} = \boldsymbol{S}_j(t_{j,0}) = \begin{bmatrix} \boldsymbol{E}_{j,0} \\ \boldsymbol{q}_j \end{bmatrix} \quad \text{with } \boldsymbol{E}_{j,0} = [n\ a_f\ a_g\ \chi\ \psi\ \lambda_M]_{j,0}^T \quad \text{and} \quad \boldsymbol{q}_j = [b\ \ c]_j^T \tag{9}$$

with the index j indicating either the primary satellite, $j = 1$, or the secondary, $j = 2$ (a notation used throughout this analysis). The first subcomponent, $\boldsymbol{E}_{j,0}$, is a 6×1 vector of initial equinoctial orbital elements [23,30,31]. (See Ref. [31] for a detailed description of these equinoctial elements and their relationships to other orbital state representations.) The second subcomponent, $\boldsymbol{q}_j$, is a 2×1 vector of time-invariant auxiliary orbital state variables: a ballistic coefficient b and a solar radiation pressure parameter c. This makes SP states $N_S \times 1$ vectors with dimension $N_S = 6 + N_q$, or typically $N_S = 8$. (Note that this representative form for $\boldsymbol{q}_j$ will be used throughout this analysis. Many ASW OD solutions used for orbital trajectory prediction have this form, but many have $N_q = 1$, as they use only b or c as an auxiliary state variable.)

The joint PDF for the initial states $\rho_0(\boldsymbol{S}_{1,0}, \boldsymbol{S}_{2,0})$ can be expressed as the product of a marginalized and a conditional PDF [25]: $\rho_0(\boldsymbol{S}_{1,0}, \boldsymbol{S}_{2,0}) = \rho_{1,0}(\boldsymbol{S}_{1,0})\rho_{2,0}(\boldsymbol{S}_{2,0}|\boldsymbol{S}_{1,0})$. If the initial state distributions are approximately statistically independent, then $\rho_{2,0}(\boldsymbol{S}_{2,0}|\boldsymbol{S}_{1,0}) \approx \rho_{2,0}(\boldsymbol{S}_{2,0})$. Section VII employs this type of approximation when deriving the from-TCA collision rate given by Eq. (8), but also provides a method of correcting for the effects of statistical cross correlations caused by global atmospheric density forecast errors [39]. More generalized fully coupled joint PDFs that are not statistically independent can be studied in the future using a similar methodology as presented here.

This analysis assumes that the initial state PDF for each object can be expressed as a multivariate normal (MVN) function:

$$\rho_{j,0}(\boldsymbol{S}_{j,0}) = \mathcal{N}\left(\boldsymbol{S}_{j,0}, \bar{\boldsymbol{S}}_{j,0}, \bar{\mathbb{P}}_{j,0}\right) \tag{10}$$

with $\bar{\boldsymbol{S}}_{j,0}$ denoting the mean initial state vector for satellite j, and $\bar{\mathbb{P}}_{j,0}$ the associated $N_S \times N_S$ covariance matrix. The MVN function

$$\mathcal{N}\left(\boldsymbol{S}, \bar{\boldsymbol{S}}, \bar{\mathbb{P}}\right) = \left[\det(2\pi\bar{\mathbb{P}})\right]^{-1/2}\left[\exp\left(-\frac{(\boldsymbol{S}-\bar{\boldsymbol{S}})^T\,\bar{\mathbb{P}}^{-1}(\boldsymbol{S}-\bar{\boldsymbol{S}})}{2}\right)\right] \tag{11}$$

represents a PDF expressed as a single Gaussian function. Advanced OD analyses could conceivably provide $\rho_{1,0}$ and $\rho_{2,0}$ each as a Gaussian mixture model (GMM) distribution (i.e., a weighted sum of multiple MVN functions) [14,38]. In this case, the expressions presented in this study apply to each component arising from the GMM summations.

B. Propagated Orbital States and Uncertainties

Initial SP states can be propagated using numerical integration to predict future SP states [8,9], a process represented in functional form as follows:

$$\boldsymbol{S}_j(t) = \boldsymbol{\mathcal{S}}(\boldsymbol{S}_{j,0}, t_{j,0}, t) \tag{12}$$

Specifically, the function $\boldsymbol{\mathcal{S}}$ represents the nonlinear process that propagates an initial SP state $\boldsymbol{S}_{j,0}$ from an initial time $t_{j,0}$ to a future time t. (The propagation function $\boldsymbol{\mathcal{S}}$ also depends on a large ensemble of model and environmental data, collectively represented by the set $\mathcal{D}$, described in detail previously for the ASW system [8].) The function $\boldsymbol{\mathcal{S}}$ is assumed to provide a continuous one-to-one mapping of initial states $\boldsymbol{S}_{j,0}$ to future states $\boldsymbol{S}_j(t)$.

This analysis denotes SP states propagated from the mean OD epoch state as

$$\bar{\boldsymbol{S}}_j(t) = \boldsymbol{\mathcal{S}}(\bar{\boldsymbol{S}}_{j,0}, t_{j,0}, t) \tag{13}$$

The associated SP state covariance matrix can be propagated approximately as follows [2,40]:

$$\bar{\mathbb{P}}_j(t) \approx [\boldsymbol{\Psi}_j(t, t_{j,0})]\bar{\mathbb{P}}_{j,0}[\boldsymbol{\Psi}_j(t, t_{j,0})]^T + \mathbb{Q}_j(t, t_{j,0}) \tag{14}$$

with the state transition matrix (STM) comprising an $N_S \times N_S$ matrix of partial derivatives

$$\boldsymbol{\Psi}_j(t, t_{j,0}) = \left(\frac{\partial \boldsymbol{\mathcal{S}}(\boldsymbol{S}_{j,0}, t_{j,0}, t)}{\partial \boldsymbol{S}_{j,0}}\right)_{\boldsymbol{S}_{j,0}=\bar{\boldsymbol{S}}_{j,0}} \tag{15}$$

The process noise matrix $\mathbb{Q}_j(t, t_{j,0})$ improves covariance realism by accounting for errors in state modeling and propagation. For conjunction prediction and risk analysis, $\mathbb{Q}_j(t, t_{j,0})$ can be estimated using an empirically calibrated state noise compensation technique [40,41].

Notably, the ASW system does not employ a process noise matrix for covariance propagation, but instead uses a dynamic consider parameter (DCP) methodology [39], which improves covariance realism for low-Earth-orbit (LEO) satellites by dividing global atmospheric density and satellite-specific ballistic-coefficient errors into two independent components. The ASW system incorporates these two DCP error estimate components into the STM used for future covariance prediction, and sets the process noise matrix to zero in Eq. (14).

C. Propagated Satellite PV Vectors

Initial SP states can also be used to predict inertial PV vectors. The PV vector for satellite j predicted at time t can be represented in functional form as

$$\boldsymbol{X}_j(t) = \begin{bmatrix} \boldsymbol{r}_j(t) \\ \boldsymbol{v}_j(t) \end{bmatrix} = \boldsymbol{\mathcal{X}}_{\text{SP}}(\boldsymbol{S}_{j,0}, t_{j,0}, t) \tag{16}$$

The function $\boldsymbol{\mathcal{X}}_{\text{SP}}$ represents the combined nonlinear processes of propagating an SP state $\boldsymbol{S}_{j,0}$ from time $t_{j,0}$ to time t, and then converting the result into a PV vector expressed within the desired inertial frame of reference. (The function $\boldsymbol{\mathcal{X}}_{\text{SP}}$ also depends on the propagation model and environmental data $\mathcal{D}$ mentioned previously.) Given the initial quantities $\boldsymbol{S}_{j,0}$ and $t_{j,0}$, the predicted satellite trajectory represented by Eq. (16) can be calculated deterministically. This analysis denotes the PV state propagated from the mean initial orbital state as

$$\bar{\boldsymbol{X}}_j(t) = \begin{bmatrix} \bar{\boldsymbol{r}}_j(t) \\ \bar{\boldsymbol{v}}_j(t) \end{bmatrix} = \boldsymbol{\mathcal{X}}_{\text{SP}}\left(\bar{\boldsymbol{S}}_{j,0}, t_{j,0}, t\right) \tag{17}$$

D. Relative PV State

The relative PV vector defined in Eq. (4) is an important variable used to formulate collision rates and probabilities [3–5,10,13,22]. For generic trajectories, this relative PV vector can be expressed as a function of time, $\boldsymbol{X}(t)$. For SP trajectories, it can be written as the difference of two propagation functions as follows:

$$\boldsymbol{X}(t) = \boldsymbol{X}_{\text{SP}}(t, \boldsymbol{S}_{1,0}, \boldsymbol{S}_{2,0}) = \boldsymbol{\mathcal{X}}_{\text{SP}}(\boldsymbol{S}_{2,0}, t_{2,0}, t) - \boldsymbol{\mathcal{X}}_{\text{SP}}(\boldsymbol{S}_{1,0}, t_{1,0}, t) \tag{18}$$

The function $\boldsymbol{X}_{\text{SP}}$ is expressed with the initial times $t_{1,0}$ and $t_{2,0}$ suppressed for brevity.

V. Deterministic Collision Rate

The collision rate for two satellites with a deterministic relative trajectory $\boldsymbol{X} = \boldsymbol{X}(t)$ has been derived previously [22]. In summary, the derivation mathematically idealizes a collision as occurring whenever the spheres circumscribing the satellites begin to overlap as they approach one another, and then calculates the rate that such ingress events occur. For spheres idealized as empty, each ingress event typically precedes an egress event, and curved trajectories may lead to additional ingress/egress events. Linear deterministic trajectories, however, create at most one ingress event.

The derivation begins by defining the deterministic overlap status [22], or, equivalently, the binary overlap number, using a unit step function:

$$N_o^D(\boldsymbol{X}) = U(R^2 - |\boldsymbol{r}|^2) \qquad \text{with } U(x) = \begin{cases} 0 & \text{if } x \le 0 \\ 1 & \text{if } x > 0 \end{cases} \tag{19}$$

where $R = R_1 + R_2$ denotes the combined circumscribing radii of the two satellites. [Note that, for brevity, the time variable t has been temporarily suppressed. Also, $N_o^D(\boldsymbol{X})$ is expressed here in terms of $\boldsymbol{r} = \boldsymbol{r}_2 - \boldsymbol{r}_1$, the relative position subcomponent of $\boldsymbol{X}$ defined in Eq. (4); other functions of $\boldsymbol{X}$ will be similarly expressed in terms of both $\boldsymbol{r}$ and $\boldsymbol{v}$.] The time derivative of N_o^D can be derived using the chain rule [33] and simplified as follows:

$$\dot{N}_o^D(\boldsymbol{X}) = \delta(R^2 - |\boldsymbol{r}|^2)\left[\frac{d(R^2 - |\boldsymbol{r}|^2)}{dt}\right] = \delta(R^2 - |\boldsymbol{r}|^2)[-2(\boldsymbol{r}\cdot\boldsymbol{v})] \tag{20}$$

The result contains a Dirac delta function [32,33] (i.e., the unit impulse function), which represents the derivative of the unit step function: $\delta(x) = dU(x)/dx$. The rate $\dot{N}_o^D(\boldsymbol{X})$ accounts for all potential changes in the overlap status of the spheres, including ingress events that occur as the two approach one another (characterized by $\boldsymbol{r}\cdot\boldsymbol{v} < 0$), as well as egress or grazing events (with $\boldsymbol{r}\cdot\boldsymbol{v} \ge 0$).

The deterministic collision rate can be expressed similarly, but includes only ingress events [22]:

$$\dot{N}_c^D(\boldsymbol{X}) = \delta(R^2 - |\boldsymbol{r}|^2)[-2(\boldsymbol{r}\cdot\boldsymbol{v})]_+ \tag{21}$$

where the $+$ subscript denotes the nonnegativity operator: $[x]_+ = x\ U(x) = \max(0, x)$. This rate would be expected for the idealized case of two perfectly tracked satellites, and the delta function reflects the discrete, instantaneous nature of ingress events between the two circumscribing spheres.

The deterministic collision rate can be written in a different form by examining the time dependence of the argument of the delta function: $F_o(t) = R^2 - |\boldsymbol{r}(t)|^2$. All of the real-valued roots of the function $F_o(t)$ within the interval $\tau_a \le t < \tau_b$ can be grouped into two sets, $\{\mathfrak{t}_i, i = 1, \ldots, I\}$ and $\{\mathfrak{t}_e, e = 1, \ldots, E\}$, representing ingresses and egresses/grazes, respectively. (These are empty sets if $I = 0$ or $E = 0$, and otherwise assumed to be time ordered so that $\mathfrak{t}_i < \mathfrak{t}_{i+1}$.) The delta function in Eq. (21) can be expressed as a sum over all of these roots [33] using a separate summation for each set:

$$\delta(R^2 - |\boldsymbol{r}(t)|^2) = \sum_{i=1}^{I} \frac{\delta(t - \mathfrak{t}_i)}{2|\boldsymbol{r}(\mathfrak{t}_i)\cdot\boldsymbol{v}(\mathfrak{t}_i)|} - \sum_{e=1}^{E} \frac{\delta(t - \mathfrak{t}_e)}{2|\boldsymbol{r}(\mathfrak{t}_e)\cdot\boldsymbol{v}(\mathfrak{t}_e)|} \tag{22}$$

(Summations of this type are defined to be zero if $I = 0$ or $E = 0$.) Inserting this into Eq. (21) and simplifying yield an alternative expression for the deterministic collision rate:

$$\dot{N}_c^D(\boldsymbol{X}(t)) = \sum_{i=1}^{I} \delta(t - \mathfrak{t}_i) \tag{23}$$

comprising a series of delta functions that occur at the ingress times. Integrating this rate over time yields the deterministic collision number:

$$N_c^D(\tau_a, t) = \int_{\tau_a}^{t} \mathrm{d}t'\ \dot{N}_c^D(\boldsymbol{X}(t')) = \sum_{i=1}^{I} U(t - \mathfrak{t}_i) \tag{24}$$

implying that the number of collisions for the entire risk-assessment interval is $N_c^D(\tau_a, \tau_b) = I$.

The deterministic collision rate $\dot{N}_c^D$ derived previously accounts for all ingresses that occur during a specified time interval, meaning that the deterministic collision number N_c^D can potentially exceed one for curved trajectories. This means that the statistically expected collision number $N_c(\tau_a, \tau_b)$ calculated using Eq. (2) can also potentially exceed one. However, the corresponding collision probability $P_c(\tau_a, \tau_b)$ calculated using Eq. (1) cannot exceed one, and so must be formulated differently. To account for this difference, P_c calculations need to include only "first-contact" collision events [8]. Specifically, a first-contact collision represents the earliest ingress that occurs during the interval $\tau_a \le t < \tau_b$ for the deterministic relative trajectory $\boldsymbol{X}(t)$. The probability rate equals the expected rate of first-contact collisions: $\dot{P}_c(t) = \mathbb{E}[\dot{N}_{\mathrm{fc}}^D(t)]$. This adjustment limits collision probabilities calculated using Eq. (1) to the appropriate range of $0 \le P_c(\tau_a, \tau_b) \le 1$. The rate that first-contact collisions occur for a deterministic trajectory $\boldsymbol{X}(t)$ can be expressed in two equivalent forms:

$$\dot{N}_{\mathrm{fc}}^D(t) = [1 - U(N_c^D(\tau_a, t))]\dot{N}_c^D(\boldsymbol{X}(t)) = \begin{cases} 0 & \text{if } I = 0 \\ \delta(t - \mathfrak{t}_1) & \text{if } I > 0 \end{cases} \tag{25}$$

The factor in the square brackets in Eq. (25) equals zero for all times after the first ingress. Notably, this factor cannot be expressed in terms of $\boldsymbol{X}(t)$ alone; instead, it depends on the entire preceding trajectory $\boldsymbol{X}(t')$ spanning $\tau_a \le t' < t$. This specific factor prevents the separation of collision probabilities into multiple time segments that can be calculated and summed independently. The second form of $\dot{N}_{\mathrm{fc}}^D$ shown in Eq. (25) includes only the first ingress from Eq. (23), if any exist. Integrating this over time yields the deterministic first-contact collision number:

$$N_{\mathrm{fc}}^D(\tau_a, t) = \begin{cases} 0 & \text{if } I = 0 \\ U(t - \mathfrak{t}_1) & \text{if } I > 0 \end{cases} \tag{26}$$

implying that $N_{\mathrm{fc}}^D(\tau_a, \tau_b) = U(I)$.

VI. MC Collision Rates and Probabilities

The expected collision rate for two tracked satellites with trajectories predicted using high-fidelity SP state propagations can be expressed by combining Eqs. (3) and (18):

$$\dot{N}_c(t) = \int \mathrm{d}\boldsymbol{S}_{1,0} \int \mathrm{d}\boldsymbol{S}_{2,0} \rho_0(\boldsymbol{S}_{1,0}, \boldsymbol{S}_{2,0}) \left[\dot{N}_c^D(\boldsymbol{X}_{\mathrm{SP}}(t, \boldsymbol{S}_{1,0}, \boldsymbol{S}_{2,0}))\right] \tag{27}$$

Unfortunately, this expression cannot be evaluated analytically in a straightforward manner, because it entails two N_S-dimensional integrations over a very complicated integrand. However, it can be evaluated straightforwardly using an MC approach.

The joint PDF ρ_0 that appears in Eq. (27) can be sampled for use in an MC simulation designed to estimate collision risks [8]. Let the initial SP states sampled for the mth MC trial be denoted as $\boldsymbol{S}_{1,0}^m$ and $\boldsymbol{S}_{2,0}^m$, with $m = 1, \ldots, M$. The MC representation for the joint distribution function is given by a sum of multidimensional delta functions as follows:

$$\rho_0(\boldsymbol{S}_{1,0}, \boldsymbol{S}_{2,0}) = \frac{1}{M} \sum_{m=1}^{M} [\delta(\boldsymbol{S}_{1,0} - \boldsymbol{S}_{1,0}^m)\delta(\boldsymbol{S}_{2,0} - \boldsymbol{S}_{2,0}^m)] \tag{28}$$

Substituting this expression for the PDF in Eq. (27) allows the expectation value integrals to be evaluated analytically. Also, each pair of sampled states, $\boldsymbol{S}_{1,0}^m$ and $\boldsymbol{S}_{2,0}^m$, defines a deterministic relative trajectory, $\boldsymbol{X}(t) = \boldsymbol{X}_{\mathrm{SP}}(t, \boldsymbol{S}_{1,0}^m, \boldsymbol{S}_{2,0}^m)$, and so Eq. (23) can be used to simplify the result further, yielding the following expression for the MC collision rate:

$$\dot{N}_c^{\mathrm{MC}}(t) = \frac{1}{M} \sum_{m=1}^{M} \left[\sum_{i=1}^{I^m} \delta(t - \mathfrak{t}_i^m)\right] \tag{29}$$

where the set $\{\mathfrak{t}_i^m, i = 1, \ldots, I^m\}$ represents the ingress times for the mth MC trial that occur within $\tau_a \le t < \tau_b$. These ingress times can be determined numerically [8]. Integrating this rate over time yields the MC estimate for the expected cumulative number of collisions:

$$N_c^{\mathrm{MC}}(\tau_a, t) = \frac{1}{M} \sum_{m=1}^{M} \left[\sum_{i=1}^{I^m} U(t - \mathfrak{t}_i^m)\right] \tag{30}$$

Including only the first ingress event for each trial yields the MC collision probability expressions:

$$\dot{P}_c^{\mathrm{MC}}(t) = \frac{1}{M}\sum_{m=1}^{M}\delta(t-\mathfrak{t}_1^m) \quad \text{and} \quad P_c^{\mathrm{MC}}(\tau_a,t) = \frac{1}{M}\sum_{m=1}^{M}U(t-\mathfrak{t}_1^m) \tag{31}$$

These equations form the basis of the BFMC collision probability estimation software algorithm used by the CARA team [8,34]. Notably, this MC formulation imposes no restrictions on the duration of the risk-assessment interval, and it can be used to estimate rates and probabilities over durations that include one or more encounters between the two tracked satellites.

VII. Semi-Analytical Collision Rates for Multi-Encounter and Single-Encounter Interactions

For SP propagations, a multi-encounter interaction can be subdivided in time using the nominal separation distance, $\bar{r}(t) = |\boldsymbol{r}_{\mathrm{SP}}(\bar{\boldsymbol{S}}_{1,0}, \bar{\boldsymbol{S}}_{2,0}, t)|$, calculated from the relative position component of Eq. (18). Figure 1 plots $\bar{r}(t)$ for two GEO satellites [34], along with a 3 day risk-assessment interval $\tau_a \le t < \tau_b$ bounded by dashed lines. Expected collision rates tend to peak near the times of the minima on the $\bar{r}(t)$ curve [20], each of which represents an approach between the two satellites. Figure 1 highlights these minima with downward-pointing red triangles and the bracketing maxima with upward-pointing blue triangles. For SP propagations, these extrema can be determined numerically. Each span between successive maxima defines an encounter segment, which, by construction, contains a single approach. Any desired risk-assessment time interval can be subdivided into such encounter segments, as long as the $\bar{r}(t)$ curve varies smoothly in time. (This analysis neglects cases with constant $\bar{r}$, such as perfectly synchronized leader/trailer satellites [22], or with noisy $\bar{r}$ curves that conceivably could be produced by some propagation schemes.) Two additional extrema that occur just before τ_a and/or just after τ_b may also need to be considered to ensure that the combined segments span the entire risk-assessment interval. The example in Fig. 1 requires seven encounter segments, two of which extend beyond the dashed lines indicating τ_a and τ_b.

Let the superscript index $k = 1, \ldots, K$ denote the encounter segments with approach times T^k and bounding maxima times $T_A^k \le t < T_B^k$. High-fidelity propagations represented by Eq. (13) can be used to predict the mean SP state for each satellite at each of the approach times:

$$\bar{\boldsymbol{S}}_j(T^k) = \boldsymbol{\mathcal{S}}\big(\bar{\boldsymbol{S}}_{j,0}, t_{j,0}, T^k\big) = \begin{bmatrix} \bar{\boldsymbol{E}}_j^k \\ \bar{\boldsymbol{q}}_j \end{bmatrix} \tag{32}$$

Equation (14) can be used to calculate the associated covariance matrix:

$$\begin{aligned}\bar{\mathbb{P}}_j(T^k) &= [\boldsymbol{\Psi}_j(T^k, t_{j,0})]\bar{\mathbb{P}}_{j,0}[\boldsymbol{\Psi}_j(T^k, t_{j,0})]^T + \mathbb{Q}_j(T^k, t_{j,0}) \\ &= \begin{bmatrix} \bar{\boldsymbol{\mathcal{P}}}_j^k & [\bar{\boldsymbol{\mathcal{W}}}_j^k]^T \\ \bar{\boldsymbol{\mathcal{W}}}_j^k & \bar{\boldsymbol{\mathcal{Z}}}_j^k \end{bmatrix}\end{aligned} \tag{33}$$

which is decomposed into three submatrices: the marginalized equinoctial covariance $\bar{\boldsymbol{\mathcal{P}}}_j^k$, the marginalized auxiliary state variable covariance $\bar{\boldsymbol{\mathcal{Z}}}_j^k$, and a matrix representing cross correlations $\bar{\boldsymbol{\mathcal{W}}}_j^k$.

A. Collision Rates Approximated for a Single Encounter Using Two-Body Motion Trajectories

The next three subsections (Secs. VII.A, VII.B, and VII.C) focus on approximating collision rates for a single encounter segment and suppress the segment index k for convenience (i.e., $T^k = T$, $\bar{\boldsymbol{E}}_j^k = \bar{\boldsymbol{E}}_j$, $\bar{\boldsymbol{\mathcal{P}}}_j^k = \bar{\boldsymbol{\mathcal{P}}}_j$, etc.). For many encounters, collision risk accumulates during a relatively short duration at or near the TCA time, T [4–8,20,42]. If this duration is sufficiently short, then the trajectories during the encounter can be approximated using two-body equations of motion:

$$\boldsymbol{X}_j(t) \approx \boldsymbol{\mathcal{X}}_{\mathrm{TB}}(\boldsymbol{E}_j, T, t) \tag{34}$$

The function $\boldsymbol{\mathcal{X}}_{\mathrm{TB}}$ represents the combined nonlinear processes of propagating an equinoctial element vector $\boldsymbol{E}_j$ from T to a nearby time t using two-body equations of motion, and then converting the result into an inertial-frame PV vector. Given T and t, this function provides a continuous one-to-one mapping between the TCA equinoctial vectors, $\boldsymbol{E}_j = \boldsymbol{E}_j(T)$, and the propagated PV vectors, $\boldsymbol{X}_j(t)$, both of which have dimension 6×1. This one-to-one mapping can be inverted:

$$\boldsymbol{E}_j = \mathcal{E}_{\mathrm{TB}}(\boldsymbol{X}_j(t), t, T) \tag{35}$$

where the function $\mathcal{E}_{\mathrm{TB}}$ represents the combined nonlinear processes of propagating the PV vector $\boldsymbol{X}_j(t)$ from t to T using two-body equations of motion, and converting the result into equinoctial elements. Vallado and Alfano [31] describe detailed algorithms to calculate $\boldsymbol{\mathcal{X}}_{\mathrm{TB}}$ and $\mathcal{E}_{\mathrm{TB}}$.

For primary and secondary PDFs that are approximately Gaussian and statistically independent, the uncertainty distribution of TCA equinoctial states can be expressed as the product of the individual marginalized equinoctial PDFs:

$$\varrho(\boldsymbol{E}_1, \boldsymbol{E}_2) \approx \varrho_1(\boldsymbol{E}_1)\varrho_2(\boldsymbol{E}_2) = \mathcal{N}(\boldsymbol{E}_1, \bar{\boldsymbol{E}}_1, \bar{\boldsymbol{\mathcal{P}}}_1)\mathcal{N}(\boldsymbol{E}_2, \bar{\boldsymbol{E}}_2, \bar{\boldsymbol{\mathcal{P}}}_2) \tag{36}$$

where $\bar{\boldsymbol{E}}_j$ is the mean TCA equinoctial state for satellite j from Eq. (32), and $\bar{\boldsymbol{\mathcal{P}}}_j$ is the associated marginalized covariance from Eq. (33). Note, $\bar{\boldsymbol{E}}_j$ and $\bar{\boldsymbol{\mathcal{P}}}_j$ for both satellites can be derived by transforming the states and covariances provided within a CDM [21], as produced by the ASW system. Equation (36) approximates each PDF ϱ_j using a single MVN function. Again, for other OD methods that express these PDFs in GMM form [14,38], the expressions derived in this analysis can be applied to each resulting summation component.

The expected collision rate for a single encounter with trajectories approximated using two-body equations of motion can now be expressed in the form of Eq. (3) as follows:

$$\begin{aligned}\dot{N}_c(t) &= \mathbb{E}\big[\dot{N}_c^D(\boldsymbol{X}(t))\big] \\ &\approx \int \mathrm{d}\boldsymbol{E}_1 \int \mathrm{d}\boldsymbol{E}_2 \varrho_1(\boldsymbol{E}_1)\varrho_2(\boldsymbol{E}_2)\big[\dot{N}_c^D(\boldsymbol{X}_{\mathrm{TB}}(t, \boldsymbol{E}_1, \boldsymbol{E}_2))\big]\end{aligned} \tag{37}$$

In this case, the relative PV state represents the difference between the two-body propagations:

$$\boldsymbol{X}(t) = \boldsymbol{X}_{\mathrm{TB}}(t, \boldsymbol{E}_1, \boldsymbol{E}_2) = \boldsymbol{\mathcal{X}}_{\mathrm{TB}}(\boldsymbol{E}_2, T, t) - \boldsymbol{\mathcal{X}}_{\mathrm{TB}}(\boldsymbol{E}_1, T, t) \tag{38}$$

Equation (37) contains two 6-D integrals over equinoctial states, which can be transformed into two 6-D integrals over inertial PV vectors and then evaluated analytically using a multistep process. The first step entails approximating the nonlinear two-body motion for each satellite in Eq. (34) with a first-order series expansion of the form:

$$\boldsymbol{X}_j(t) \approx \boldsymbol{\mathcal{X}}_{\mathrm{TB}}\big(\tilde{\boldsymbol{E}}_j, T, t\big) + \left[\left(\frac{\partial \boldsymbol{\mathcal{X}}_{\mathrm{TB}}(\boldsymbol{E}_j, T, t)}{\partial \boldsymbol{E}_j}\right)_{\boldsymbol{E}_j = \tilde{\boldsymbol{E}}_j}\right]\big(\boldsymbol{E}_j - \tilde{\boldsymbol{E}}_j\big) \tag{39a}$$

$$= \tilde{\boldsymbol{X}}_j(t) + [\tilde{\boldsymbol{\Psi}}_j(t)]\big(\boldsymbol{E}_j - \tilde{\boldsymbol{E}}_j\big) \tag{39b}$$

Notably, this series expansion is not centered on the mean TCA equinoctial state, $\bar{\boldsymbol{E}}_j$, but rather a different TCA state, $\tilde{\boldsymbol{E}}_j$, which later will be selected carefully to optimize the accuracy of the first-order approximation in the region of state space most important for collision rate estimation. The Jacobian matrix of partial derivatives required for the series expansion can be expressed as the product of two 6×6 matrices:

$$\tilde{\boldsymbol{\psi}}_j(t) = \{\tilde{\boldsymbol{\alpha}}_j(t)\}[\boldsymbol{\beta}(t,T)] = \left\{\frac{\partial \tilde{\boldsymbol{X}}_j(t)}{\partial \tilde{\boldsymbol{E}}_j(t)}\right\} \begin{bmatrix} 1 & 0 & 0 & 0 & 0 & 0 \\ 0 & 1 & 0 & 0 & 0 & 0 \\ 0 & 0 & 1 & 0 & 0 & 0 \\ 0 & 0 & 0 & 1 & 0 & 0 \\ 0 & 0 & 0 & 0 & 1 & 0 \\ t-T & 0 & 0 & 0 & 0 & 1 \end{bmatrix} \tag{40}$$

The $\tilde{\boldsymbol{\alpha}}_j(t)$ matrix in curly brackets represents the two-body equinoctial-to-Cartesian transformation described in detail in Ref. [31]. The square brackets contain the two-body motion STM for equinoctial states, $\boldsymbol{\beta}(t,T) = \partial \boldsymbol{E}(t)/\partial \boldsymbol{E}(T)$, which has one nonzero off-diagonal element [9]. Reference [23] (table 1) presents an alternate formulation for $\tilde{\boldsymbol{\psi}}_j(t)$, but using the semimajor axis instead of the mean motion as the first equinoctial element.

Equation (39b) can be rearranged as follows, suppressing the variable t temporarily for convenience:

$$\boldsymbol{E}_j \approx \tilde{\boldsymbol{E}}_j + [\tilde{\boldsymbol{\psi}}_j]^{-1}\big(\boldsymbol{X}_j - \tilde{\boldsymbol{X}}_j\big) \tag{41}$$

This approximation can be used to transform the integration variables in Eq. (37) from TCA equinoctial vectors $\boldsymbol{E}_j$ to inertial-frame PV vectors $\boldsymbol{X}_j$. The multidimensional differential elements of the two integrals transform in inverse proportion to the determinant of the Jacobian matrix [18,33]:

$$d\boldsymbol{E}_j = d\boldsymbol{X}_j[\det(\tilde{\boldsymbol{\psi}}_j)]^{-1} = d\boldsymbol{X}_j|\tilde{\boldsymbol{\psi}}_j|^{-1} \tag{42}$$

The products $d\boldsymbol{E}_j\, \varrho_j(\boldsymbol{E}_j)$ in Eq. (37) can be transformed using the following multistep process:

$$d\boldsymbol{E}_j \varrho_j(\boldsymbol{E}_j) = d\boldsymbol{E}_j \mathcal{N}\big(\boldsymbol{E}_j, \bar{\boldsymbol{E}}_j, \bar{\boldsymbol{\mathcal{P}}}_j\big) \tag{43a}$$

$$\approx d\boldsymbol{X}_j|\tilde{\boldsymbol{\psi}}_j|^{-1}\mathcal{N}\Big(\tilde{\boldsymbol{E}}_j + \tilde{\boldsymbol{\psi}}_j^{-1}\big(\boldsymbol{X}_j - \tilde{\boldsymbol{X}}_j\big), \bar{\boldsymbol{E}}_j, \bar{\boldsymbol{\mathcal{P}}}_j\Big) \tag{43b}$$

$$= d\boldsymbol{X}_j|\tilde{\boldsymbol{\psi}}_j|^{-1}\mathcal{N}\Big(\tilde{\boldsymbol{\psi}}_j^{-1}\big(\boldsymbol{X}_j - \tilde{\boldsymbol{X}}_j\big), \bar{\boldsymbol{E}}_j - \tilde{\boldsymbol{E}}_j, \bar{\boldsymbol{\mathcal{P}}}_j\Big) \tag{43c}$$

$$= d\boldsymbol{X}_j\, \mathcal{N}\Big(\boldsymbol{X}_j - \tilde{\boldsymbol{X}}_j, \tilde{\boldsymbol{\psi}}_j\big(\bar{\boldsymbol{E}}_j - \tilde{\boldsymbol{E}}_j\big), \tilde{\boldsymbol{\psi}}_j \bar{\boldsymbol{\mathcal{P}}}_j \tilde{\boldsymbol{\psi}}_j^T\Big) \tag{43d}$$

$$= d\boldsymbol{X}_j\, \mathcal{N}\big(\boldsymbol{X}_j, \check{\boldsymbol{X}}_j, \tilde{\boldsymbol{P}}_j\big) \tag{43e}$$

with the final form expressed using the following definitions:

$$\check{\boldsymbol{X}}_j = \tilde{\boldsymbol{X}}_j + \tilde{\boldsymbol{\psi}}_j\big(\bar{\boldsymbol{E}}_j - \tilde{\boldsymbol{E}}_j\big) = \begin{bmatrix} \check{\boldsymbol{r}}_j \\ \check{\boldsymbol{v}}_j \end{bmatrix} \quad \text{and } \tilde{\boldsymbol{P}}_j = \tilde{\boldsymbol{\psi}}_j \bar{\boldsymbol{\mathcal{P}}}_j \tilde{\boldsymbol{\psi}}_j^T = \begin{bmatrix} \tilde{\boldsymbol{A}}_j & \tilde{\boldsymbol{B}}_j^T \\ \tilde{\boldsymbol{B}}_j & \tilde{\boldsymbol{C}}_j \end{bmatrix} \tag{44}$$

and with the PV covariance matrix $\tilde{\boldsymbol{P}}_j$ decomposed into three submatrices: the marginalized position covariance $\tilde{\boldsymbol{A}}_j$, the marginalized velocity covariance $\tilde{\boldsymbol{C}}_j$, and a cross-correlation matrix $\tilde{\boldsymbol{B}}_j$. Both $\check{\boldsymbol{X}}_j$ and $\tilde{\boldsymbol{P}}_j$ depend on time.

Equation (43e) indicates that the first-order approximation for the density of PV states is $\mathcal{N}(\boldsymbol{X}_j, \check{\boldsymbol{X}}_j, \tilde{\boldsymbol{P}}_j)$. This PDF peaks in PV state space at $\check{\boldsymbol{X}}_j$, which is offset from the propagated expansion-center state $\tilde{\boldsymbol{X}}_j$. Inserting Eq. (43e) into Eq. (37) for both satellites and simplifying yield

$$\dot{N}_c(t) \approx \int d\boldsymbol{X}_1 \mathcal{N}(\boldsymbol{X}_1, \check{\boldsymbol{X}}_1, \tilde{\boldsymbol{P}}_1) \int d\boldsymbol{X}_2 \mathcal{N}(\boldsymbol{X}_2, \check{\boldsymbol{X}}_2, \tilde{\boldsymbol{P}}_2)[\dot{N}_c^D(\boldsymbol{X}_2 - \boldsymbol{X}_1)] \tag{45}$$

The integration over $\boldsymbol{X}_2$ can be transformed to one over $\boldsymbol{X} = \boldsymbol{X}_2 - \boldsymbol{X}_1$, allowing the expression to be simplified further using a multistep process summarized as follows:

$$\dot{N}_c(t) \approx \int d\boldsymbol{X}_1 \mathcal{N}\big(\boldsymbol{X}_1, \check{\boldsymbol{X}}_1, \tilde{\boldsymbol{P}}_1\big) \int d\boldsymbol{X} \mathcal{N}\big(\boldsymbol{X} + \boldsymbol{X}_1, \check{\boldsymbol{X}}_2, \tilde{\boldsymbol{P}}_2\big)\big[\dot{N}_c^D(\boldsymbol{X})\big] \tag{46a}$$

$$= \int d\boldsymbol{X}\big[\dot{N}_c^D(\boldsymbol{X})\big] \int d\boldsymbol{X}_1 \mathcal{N}\big(\boldsymbol{X}_1, \check{\boldsymbol{X}}_1, \tilde{\boldsymbol{P}}_1\big)\mathcal{N}\big(\boldsymbol{X} + \boldsymbol{X}_1, \check{\boldsymbol{X}}_2, \tilde{\boldsymbol{P}}_2\big) \tag{46b}$$

$$= \int d\boldsymbol{X}\big[\dot{N}_c^D(\boldsymbol{X})\big] \int d\boldsymbol{X}_1 \mathcal{N}\big(\boldsymbol{X}_1, \check{\boldsymbol{X}}_1, \tilde{\boldsymbol{P}}_1\big)\mathcal{N}\big(\boldsymbol{X}_1, \check{\boldsymbol{X}}_2 - \boldsymbol{X}, \tilde{\boldsymbol{P}}_2\big) \tag{46c}$$

$$= \int d\boldsymbol{X} \mathcal{N}\big(\check{\boldsymbol{X}}_1, \check{\boldsymbol{X}}_2 - \boldsymbol{X}, \tilde{\boldsymbol{P}}_1 + \tilde{\boldsymbol{P}}_2\big)\big[\dot{N}_c^D(\boldsymbol{X})\big]\left\{\int d\boldsymbol{X}_1 \mathcal{N}(\boldsymbol{X}_1, \boldsymbol{\mu}', \boldsymbol{\Sigma}')\right\} \tag{46d}$$

$$= \int d\boldsymbol{X} \mathcal{N}\big(\boldsymbol{X}, \check{\boldsymbol{X}}, \tilde{\boldsymbol{P}}\big)\big[\dot{N}_c^D(\boldsymbol{X})\big] \tag{46e}$$

with the final form expressed using the following definitions:

$$\check{\boldsymbol{X}} = \check{\boldsymbol{X}}_2 - \check{\boldsymbol{X}}_1 = \begin{bmatrix} \check{\boldsymbol{r}} \\ \check{\boldsymbol{v}} \end{bmatrix} \quad \text{and} \quad \tilde{\boldsymbol{P}} = \tilde{\boldsymbol{P}}_1 + \tilde{\boldsymbol{P}}_2 = \begin{bmatrix} \tilde{\boldsymbol{A}} & \tilde{\boldsymbol{B}}^T \\ \tilde{\boldsymbol{B}} & \tilde{\boldsymbol{C}} \end{bmatrix} \tag{47}$$

Transforming Eq. (46c) into Eq. (46d) uses the formula for the product of two MVN functions [43]:

$$\begin{aligned} &\mathcal{N}(\boldsymbol{X}_1, \check{\boldsymbol{X}}_1, \tilde{\boldsymbol{P}}_1)\mathcal{N}(\boldsymbol{X}_1, \check{\boldsymbol{X}}_2 - \boldsymbol{X}, \tilde{\boldsymbol{P}}_2) \\ &\quad = \mathcal{N}(\check{\boldsymbol{X}}_1, \check{\boldsymbol{X}}_2 - \boldsymbol{X}, \tilde{\boldsymbol{P}}_1 + \tilde{\boldsymbol{P}}_2)\mathcal{N}(\boldsymbol{X}_1, \boldsymbol{\mu}', \boldsymbol{\Sigma}') \end{aligned} \tag{48}$$

This produces the integral shown in curly brackets in Eq. (46d), which equals 1. The PDF $\mathcal{N}(\boldsymbol{X}, \check{\boldsymbol{X}}, \tilde{\boldsymbol{P}})$ in Eq. (46e) can be expressed as a product of a marginalized relative position PDF and a conditional relative velocity PDF [43]:

$$\mathcal{N}(\boldsymbol{X}, \check{\boldsymbol{X}}, \tilde{\boldsymbol{P}}) = \mathcal{N}(\boldsymbol{r}, \check{\boldsymbol{r}}, \tilde{\boldsymbol{A}})\mathcal{N}(\boldsymbol{v}, \check{\boldsymbol{v}}', \tilde{\boldsymbol{C}}') \tag{49}$$

with

$$\check{\boldsymbol{v}}' = \boldsymbol{v} + \tilde{\boldsymbol{B}}\tilde{\boldsymbol{A}}^{-1}(\boldsymbol{r} - \check{\boldsymbol{r}}) \qquad \text{and} \qquad \tilde{\boldsymbol{C}}' = \tilde{\boldsymbol{C}} - \tilde{\boldsymbol{B}}\tilde{\boldsymbol{A}}^{-1}\tilde{\boldsymbol{B}}^T \tag{50}$$

These expressions allow the 6-D integral over $\boldsymbol{X}$ in Eq. (46e) to be separated into two 3-D integrals over $\boldsymbol{r}$ and $\boldsymbol{v}$, which can be combined with Eq. (21) and simplified as follows:

$$\dot{N}_c(t)$$

$$\approx \int d\boldsymbol{r} \mathcal{N}\big(\boldsymbol{r}, \check{\boldsymbol{r}}, \tilde{\boldsymbol{A}}\big)\{\delta(R^2 - |\boldsymbol{r}|^2)\} \int d\boldsymbol{v} \mathcal{N}\big(\boldsymbol{v}, \check{\boldsymbol{v}}', \tilde{\boldsymbol{C}}'\big)[-2(\boldsymbol{r}\cdot\boldsymbol{v})]_+ \tag{51a}$$

$$= \int dr\, r^2\{\delta(R^2 - r^2)\} \oint d\hat{\boldsymbol{r}} \mathcal{N}\big(r\hat{\boldsymbol{r}}, \check{\boldsymbol{r}}, \tilde{\boldsymbol{A}}\big) \int d\boldsymbol{v} \mathcal{N}\big(\boldsymbol{v}, \check{\boldsymbol{v}}', \tilde{\boldsymbol{C}}'\big)[-2(r\hat{\boldsymbol{r}}\cdot\boldsymbol{v})]_+ \tag{51b}$$

$$= \int dr\, r^2 \left\{\frac{\delta(r-R)}{2R}\right\} \oint d\hat{\boldsymbol{r}} \mathcal{N}\big(r\hat{\boldsymbol{r}}, \check{\boldsymbol{r}}, \tilde{\boldsymbol{A}}\big) \int d\boldsymbol{v} \mathcal{N}\big(\boldsymbol{v}, \check{\boldsymbol{v}}', \tilde{\boldsymbol{C}}'\big)[-2(r\hat{\boldsymbol{r}}\cdot\boldsymbol{v})]_+ \tag{51c}$$

$$= R^2 \oint d\hat{\boldsymbol{r}} \mathcal{N}\big(R\hat{\boldsymbol{r}}, \check{\boldsymbol{r}}, \tilde{\boldsymbol{A}}\big)\left\{\int d\boldsymbol{v} \mathcal{N}\big(\boldsymbol{v}, \check{\boldsymbol{v}}', \tilde{\boldsymbol{C}}'\big)[-(\hat{\boldsymbol{r}}\cdot\boldsymbol{v})]_+\right\} \tag{51d}$$

$$= R^2 \oint d\hat{\boldsymbol{r}} \mathcal{N}\big(R\hat{\boldsymbol{r}}, \check{\boldsymbol{r}}, \tilde{\boldsymbol{A}}\big)\{\nu(\hat{\boldsymbol{r}}, \check{\boldsymbol{X}}, \tilde{\boldsymbol{P}})\} \tag{51e}$$

For this, the integral over $\boldsymbol{r}$ in Eq. (51a) has been transformed using spherical coordinates [33], and the associated differential element expressed as $d\boldsymbol{r} = (dr\ r^2)d\hat{\boldsymbol{r}}$, with $d\hat{\boldsymbol{r}}$ denoting a differential area on the unit sphere and $\oint d\hat{\boldsymbol{r}}$ integration over the full unit sphere. Equation (51c) transforms the delta function [33] as $\delta(R^2 - r^2) = \delta(r - R)/(2R)$, which allows analytical evaluation of the integral over r. The integral over relative velocity in the curly brackets in Eq. (51d) has been evaluated previously [13]:

$$\nu(\hat{\boldsymbol{r}}, \check{\boldsymbol{X}}, \tilde{\boldsymbol{P}}) = \frac{\sigma}{\sqrt{2\pi}} H(\tilde{\nu}) \qquad \text{with } \sigma = \sqrt{\hat{\boldsymbol{r}}^T \tilde{\boldsymbol{C}}' \hat{\boldsymbol{r}}} \quad \text{and} \tag{52a}$$

$$H(\tilde{\nu}) = e^{-\tilde{\nu}^2} - \sqrt{\pi}\tilde{\nu}\ \mathrm{erfc}(\tilde{\nu}) \qquad \text{and} \quad \tilde{\nu} = \frac{\hat{\boldsymbol{r}}\left[\check{\boldsymbol{v}} + \tilde{\boldsymbol{B}}\tilde{\boldsymbol{A}}^{-1}(R\hat{\boldsymbol{r}} - \check{\boldsymbol{r}})\right]}{\sqrt{2}\sigma} \tag{52b}$$

which uses the complementary error function, $\mathrm{erfc}(\tilde{\nu}) = 1 - \mathrm{erf}(\tilde{\nu})$. Because $\check{\boldsymbol{X}}$ and $\tilde{\boldsymbol{P}}$ and their subcomponents depend on time, the integral given by Eq. (51e) implicitly does also.

B. Finding the Center States for the First-Order Taylor Series Expansion

The TCA equinoctial states $\tilde{\boldsymbol{E}}_1$ and $\tilde{\boldsymbol{E}}_2$ used as the center points for the first-order series expansion of Eqs. (39) and (41) have yet to be specified. This section develops a method of selecting these "expansion-center" states optimized for accurate collision rate estimation. As discussed by Shelton and Junkins [18], the primary and secondary PDFs optimally should be estimated accurately in the volume where they overlap the most (see fig. 2 of Ref. [18]). The peak-overlap location occurs where the product of the two position PDFs is maximum. This formulation selects expansion-center states that coincide with this peak-overlap location, which requires an iterative calculation to determine. Also, because the peak-overlap location changes as the two PDFs move and evolve, this iterative process must be performed each time $\dot{N}_c(t)$ is calculated, as described as follows.

For a given time t, Eq. (43e) provides the first-order approximation for the density of PV states for satellite j, $\mathcal{N}(\boldsymbol{X}_j, \check{\boldsymbol{X}}_j, \tilde{\boldsymbol{P}}_j)$, which can be expressed equivalently as a product of a marginalized position PDF and a conditional velocity PDF [43]:

$$\mathcal{N}\left(\boldsymbol{X}_j, \check{\boldsymbol{X}}_j, \tilde{\boldsymbol{P}}_j\right) = \mathcal{N}\left(\boldsymbol{r}_j, \check{\boldsymbol{r}}_j, \tilde{\boldsymbol{A}}_j\right)\mathcal{N}\left(\boldsymbol{v}_j, \check{\boldsymbol{v}}'_j, \tilde{\boldsymbol{C}}'_j\right) \tag{53}$$

where $\check{\boldsymbol{v}}'_j$ and $\tilde{\boldsymbol{C}}'_j$ are given by Eq. (50), but with the subscript j added to the components. This implies that the marginalized spatial density of primary states at an inertial position $\boldsymbol{a}$ is $\mathcal{N}(\boldsymbol{a}, \check{\boldsymbol{r}}_1, \tilde{\boldsymbol{A}}_1)$, to first-order accuracy. The density of secondary states at the same position is approximately $\mathcal{N}(\boldsymbol{a}, \check{\boldsymbol{r}}_2, \tilde{\boldsymbol{A}}_2)$. The product of these two PDFs can be expressed as [43]

$$\mathcal{N}(\boldsymbol{a}, \check{\boldsymbol{r}}_1, \tilde{\boldsymbol{A}}_1)\mathcal{N}(\boldsymbol{a}, \check{\boldsymbol{r}}_2, \tilde{\boldsymbol{A}}_2) = \mathcal{N}(\check{\boldsymbol{r}}_1, \check{\boldsymbol{r}}_2, \tilde{\boldsymbol{A}})\mathcal{N}(\boldsymbol{a}, \boldsymbol{\mu}_p, \boldsymbol{\Sigma}_p) \tag{54}$$

where $\tilde{\boldsymbol{A}} = \tilde{\boldsymbol{A}}_1 + \tilde{\boldsymbol{A}}_2$ is the joint position covariance defined in Eq. (47), and

$$\boldsymbol{\Sigma}_p = \boldsymbol{\Sigma}_p(t) = \left(\tilde{\boldsymbol{A}}_1^{-1} + \tilde{\boldsymbol{A}}_2^{-1}\right)^{-1} \qquad \text{and}$$
$$\boldsymbol{\mu}_p = \boldsymbol{\mu}_p(t) = \boldsymbol{\Sigma}_p\left(\tilde{\boldsymbol{A}}_1^{-1}\check{\boldsymbol{r}}_1 + \tilde{\boldsymbol{A}}_2^{-1}\check{\boldsymbol{r}}_2\right) \tag{55}$$

The PDF product therefore maximizes at the position $\boldsymbol{a} = \boldsymbol{\mu}_p(t)$, which represents the first-order estimate of the peak-overlap location (i.e., the mode of the joint position distribution). The covariance matrix $\boldsymbol{\Sigma}_p(t)$ provides an estimate of the extent and orientation of the joint position distribution.

Notably, the process used to generate the estimate $\boldsymbol{\mu}_p$ employs the first-order expansions of Eqs. (39) and (41), and therefore relies on having initial estimates for the expansion-center states. For this reason, this formulation uses an iterative process to find $\boldsymbol{\mu}_p$, starting with the mean states as initial estimates. At each iteration, the peak-overlap location is updated and adopted as the next expansion-center position for both satellites. As iterations continue, $\boldsymbol{\mu}_p$ converges to an increasingly accurate estimate of the actual peak-overlap location of the primary and secondary PDFs. The covariance $\boldsymbol{\Sigma}_p$ is used to assess iterative convergence. The velocity components of the expansion-center states are selected to be equal to the mean velocities of each distribution at the peak-overlap location $\boldsymbol{\mu}_p$ (i.e., the conditional velocities), yielding

$$\tilde{\boldsymbol{X}}_j = \begin{bmatrix} \boldsymbol{\mu}_p \\ \tilde{\boldsymbol{v}}_j \end{bmatrix} \qquad \text{with} \quad \tilde{\boldsymbol{v}}_j = \check{\boldsymbol{v}}_j + \tilde{\boldsymbol{B}}_j\tilde{\boldsymbol{A}}_j^{-1}(\boldsymbol{\mu}_p - \check{\boldsymbol{r}}_j) \tag{56}$$

The following step-by-step algorithm calculates the expansion-center states for a given time t:

1) Let the superscript index $\imath$ denote iterations, initialized to zero. Initialize the expansion-center TCA equinoctial states using the mean states: $\tilde{\boldsymbol{E}}_j^{\imath=0} = \bar{\boldsymbol{E}}_j(T)$ (again, j equals 1 or 2). If necessary, use Eq. (34) to propagate these from the TCA time T to the nearby time t to initialize the corresponding PV states: $\tilde{\boldsymbol{X}}_j^{\imath=0}(t) = \bar{\boldsymbol{X}}_j(t)$.

2) Increment the iteration counter $\imath$.

3) Use the previous expansion-center estimates $\{\tilde{\boldsymbol{E}}_j^{\imath-1}, \tilde{\boldsymbol{X}}_j^{\imath-1}(t)\}$ along with Eqs. (39) and (40) to calculate the next iterative estimates for the two Jacobian matrices, $\tilde{\boldsymbol{\psi}}_j^{\imath}(t)$.

4) Use Eq. (44) to calculate the next estimates for the two vectors, $\check{\boldsymbol{X}}_j^{\imath}(t)$, and two covariances, $\tilde{\boldsymbol{P}}_j^{\imath}(t)$, thereby defining the associated subcomponents $\check{\boldsymbol{r}}_j^{\imath}$, $\check{\boldsymbol{v}}_j^{\imath}$, $\tilde{\boldsymbol{A}}_j^{\imath}$, $\tilde{\boldsymbol{B}}_j^{\imath}$, and $\tilde{\boldsymbol{C}}_j^{\imath}$.

5) Use Eq. (55) to calculate the next estimate of the peak-overlap location, $\boldsymbol{\mu}_p^{\imath}(t)$.

6) Use Eq. (56) to calculate the next estimates for the two expansion-center PV states, $\tilde{\boldsymbol{X}}_j^{\imath}(t)$.

7) Use Eq. (35) to calculate the next estimates for the expansion-center TCA equinoctial states, $\tilde{\boldsymbol{E}}_j^{\imath}$.

8) For $\imath > 1$, check for convergence by examining the difference $\Delta\boldsymbol{\mu}_p = \boldsymbol{\mu}_p^{\imath} - \boldsymbol{\mu}_p^{\imath-1}$. Specifically, if the dimensionless scalar quantity $\Delta\boldsymbol{\mu}_p^T[\boldsymbol{\Sigma}_p^{\imath}]^{-1}\Delta\boldsymbol{\mu}_p$ becomes sufficiently small (e.g., $\leq 10^{-6}$), the process can be considered converged. For $\imath = 1$, continue iterating unless forcibly stopped.

9) Repeat steps 2–8 until convergence is achieved, or until $\imath$ equals the maximum allowable number of iterations (e.g., 100). For well-tracked objects, the process typically requires two to five iterations to converge.

For temporally isolated encounters, the expected collision rate given by Eq. (51e) equals the collision probability rate. Notably, this expression has the same form as the probability rate derived in the original 3-D P_c formulation [13], but the arguments used in the integrand functions are different. Specifically, the original 3-D P_c integrand factors, $\mathcal{N}(R\hat{\boldsymbol{r}}, \bar{\boldsymbol{r}}, \bar{\boldsymbol{A}})\{\nu(\hat{\boldsymbol{r}}, \bar{\boldsymbol{X}}, \bar{\boldsymbol{P}})\}$, represent the approximation obtained by forcibly stopping this algorithm after the first iteration (i.e., at $\imath = 1$ in step 8). In other words, the 3-D P_c integrand uses the mean states $\bar{\boldsymbol{E}}_1$ and $\bar{\boldsymbol{E}}_2$ as the center points for the first-order Taylor series of Eqs. (39) and (41), with no further refinement. The 3-D N_c formulation improves the accuracy of these first-order approximations by using the iteratively refined states $\tilde{\boldsymbol{E}}_1$ and $\tilde{\boldsymbol{E}}_2$ as the centers of linearization, as described previously. This specific difference explains the relatively poor agreement observed between P_c estimates from MC simulations and those from the CDM-based software implementation of CARA [20] of the original 3-D P_c method.

C. Correcting for Cross Correlations Between Single-Encounter Covariance Matrices

As mentioned previously, the ASW system uses a DCP technique to improve covariance realism for conjunctions between LEO satellites. Specifically, the DCP methodology divides atmospheric density and ballistic errors into two independent components [39]. The first represents the often predominant error due to inaccuracies in forecast

solar activity levels, which cause inaccuracies in estimated atmospheric densities [9,28,29]. The second represents error due to changes in the projected frontal area of each satellite relative to that predicted by the ballistic coefficient of the OD solution. The first DCP component is globally driven, whereas the second is satellite specific. The globally driven component creates cross correlation of orbital error between LEO satellites, which can significantly affect collision risk assessments for conjunctions that occur at lower altitudes [39]. Analysis indicates that the methodology of Casali et al. [39] can be used to show that the cross-correlation effect can be corrected in the 3-D N_c formulation by replacing the relative covariance matrix $\tilde{\boldsymbol{P}}$ in Eqs. (51e) and (52) with a decorrelated covariance of the form:

$$\tilde{\boldsymbol{P}}_* = \tilde{\boldsymbol{P}}_1 + \tilde{\boldsymbol{P}}_2 - \sigma_{1/g}\sigma_{2/g}\left(\tilde{\boldsymbol{\Gamma}}_1\tilde{\boldsymbol{\Gamma}}_2^T + \tilde{\boldsymbol{\Gamma}}_2\tilde{\boldsymbol{\Gamma}}_1^T\right) \tag{57}$$

with $\sigma_{j/g}$ representing the empirically determined 1-sigma variation level (or intensity) of the relative atmospheric density error for satellite j, and $\tilde{\boldsymbol{\Gamma}}_j$ representing the associated sensitivity vector. Efforts are currently underway to augment CDMs produced by the ASW and CARA systems to contain the $\sigma_{j/g}$ scalar values, along with data that allow the calculation of the $\tilde{\boldsymbol{\Gamma}}_j$ sensitivity vectors, which can be described in more detail in future analyses.

D. Expected Number of Collisions for Multi-Encounter Interactions

Equation (51e) can be rewritten as Eq. (8), which expresses the expected collision rate $\dot{N}_c^k(t)$ using the previously suppressed encounter segment superscript index, k. The integral in these expressions represents 2-D integration over a unit sphere, and the integrand depends on the converged expansion-center states, as described previously. Numerical integration over the unit sphere can be calculated efficiently using Lebedev quadrature [44]. Integrating the rate $\dot{N}_c^k(t)$ over time provides the expected number of collisions for the kth encounter segment:

$$N_c^k = \int_{T_A^k}^{T_B^k} \mathrm{d}t\dot{N}_c^k(t) \tag{58}$$

These integration bounds span the entire segment (i.e., the time between two successive maxima, as illustrated in Fig. 1). However, as mentioned previously, collision rates for many (but not all) encounters become appreciable only during a relatively short duration at or near TCA.

Coppola [42] presents a method to estimate the time bounds required to achieve a desired integration accuracy for linear encounters; for nonlinear encounters, these bounds can be appropriately expanded [20] and/or determined numerically. The resulting conjunction duration bounds, T_a^k and T_b^k, measure the span during which $\dot{N}_c^k(t)$ is large enough to contribute appreciably to the integral in Eq. (58). For most CARA conjunctions, this duration is much shorter than the full encounter segment [42] (i.e., $T_b^k - T_a^k \ll T_B^k - T_A^k$). Such events can be considered temporally isolated. This may not be true, however, for some long-duration encounters with low relative velocities. For these, if T_a^k approaches T_A^k (or T_b^k approaches T_B^k), then encounter segment k potentially becomes "blended" with the preceding (or following) segment. Equation (8) may become inaccurate in these cases, and interactions involving such extended/blended events should continue to be assessed using BFMC analysis [8,34,37].

The time-integration bounds in Eq. (58) must also be adjusted to account for the original risk-assessment interval $\tau_a \le t < \tau_b$. This leads to the following expressions for the final clipped bounds:

$$\tau_a^k = \max\left(T_A^k, T_a^k, \tau_a\right) \quad \text{and} \quad \tau_b^k = \min\left(T_B^k, T_b^k, \tau_b\right) \tag{59}$$

which can be used in Eq. (7) with the caveat that, if $\tau_a^k \ge \tau_b^k$ after the clipping process, then the expected collision number N_c^k should be set to zero. Otherwise, the resulting 1-D time integral can be evaluated numerically using trapezoidal, Simpson's rule, or other 1-D quadrature schemes [13,20].

VIII. Conclusions

The two principal quantities derived in this analysis—the statistically expected collision rate $\dot{N}_c$ and the expected number of collisions N_c—provide a means of quantifying the risk of collision between tracked satellites. For single, temporally isolated conjunctions, N_c and P_c are equal. For multi-encounter interactions, however, N_c provides an upper limit for P_c and is significantly easier to approximate semi-analytically. The expected value integrations used to calculate the collision rate $\dot{N}_c$ are performed over distributions of initial orbital states for the two interacting satellites. These initial states are random variables, and the initial distributions are time-invariant PDFs that represent uncertainties estimated from OD analyses of trajectory measurement data. In this analysis, these states are based on equinoctial orbital elements, which naturally account for the effects of curved orbital trajectories. The methodology allows the derivation of exact N_c and $\dot{N}_c$ expressions to use for MC simulations, and semi-analytical approximations applicable to most single- and multi-encounter interactions between Earth-orbiting satellites.

The 3-D N_c semi-analytical approximation for single encounters derived in this analysis has a similar form as the previously formulated 3-D P_c approximation [13] in that it can be calculated numerically as a 2-D integral over a unit sphere, nested within a 1-D time integral. However, specific terms within the integrands of the two calculations differ because the 3-D N_c approximation uses first-order series expansions centered optimally on the peak-overlap location of the PDFs for the two satellites, rather than simply centered on the mean states. Determining this peak-overlap location requires an iterative calculation, which converges quickly for temporally isolated encounters.

Using the expected number of collisions instead of the collision probability may also be useful in other applications. For instance, replacing P_c with N_c appears to lend itself to the survival analysis approach advocated in 2007 by Carpenter [37]. Another example relates to designing satellite collision risk mitigation maneuvers. These are typically optimized using a single-encounter 2-D P_c value as a metric to ensure that the planned maneuver sufficiently reduces the collision probability of the specific conjunction being mitigated. However, using the semi-analytical $N_c(\tau_a, \tau_b)$ approximation as an alternate metric could allow such maneuvers to be optimized for multi-encounter postmaneuver intervals, without resorting to computationally intensive MC estimations.

It is worth mentioning that assessing satellite collision risks by estimating statistically expected collision rates represents a generalized methodology suitable for a variety of applications. For different applications, the collision rate expression given by Eq. (3) need not employ the specific orbital state representations used in this analysis. For instance, a derivation for single encounters that employs the linear motion and other 2-D P_c method assumptions is conveniently formulated in terms of PV states instead of equinoctial elements, and yields expressions for $\dot{P}_c$ and P_c that each entails 2-D numerical integration over a unit hemisphere, rather than the full unit sphere.

The MC and semi-analytical collision rate expressions derived in this analysis both use state vectors based on equinoctial orbital elements. This choice has been shown to mitigate inaccurate modeling of orbital state uncertainties when using a single-Gaussian PDF approximation [24]. However, for advanced OD analyses that provide more realistic, non-Gaussian PDF estimates (e.g., GMM distributions), this specific choice of orbital state representation may not be required or even optimal—which may be worth investigating in future studies. Similarly, instead of using equinoctial elements, the 3-D N_c approximation derived in Sec. VII of this analysis likely could also be formulated using other two-body state representations or methods (such as "f and g" functions [9], for instance), which could potentially improve computational speed or other performance metrics.

Analysis indicates that the expected collision rate methodology also can be applied to more advanced OD solutions than considered

in this analysis (e.g., with fully coupled primary–secondary orbital states and correlated uncertainty PDFs), or even to high-fidelity state/covariance ephemerides. These applications yield expressions for N_c and $\dot{N}_c$ similar to those presented here for both single- and multi-encounter interactions.

Acknowledgments

This research was funded by the NASA Goddard Space Flight Center through the Flight Dynamics Support Services III contract (contract number 80GSFC19C0072). The author would like to thank Luis Baars, Russell Carpenter, Steve Casali, Joseph Frisbee, Matthew Hejduk, Lauren Johnson, Jon Kolb, Kenneth Kopke, Travis Lechtenberg, Brent Skrehart, and Daniel Snow for several helpful discussions and analyses.

References

[1] Newman, L. K., "The NASA Robotic Conjunction Assessment Process: Overview and Operational Experiences," *Acta Astronautica*, Vol. 66, Nos. 6–7, 2010, pp. 1253–1261. https://doi.org/10.1016/J.ACTAASTRO.2009.10.005

[2] Tapley, B. D., Schutz, B. E., and Born, G. H., *Statistical Orbit Determination*, Elsevier, Burlington, MA, 2004, Chaps. 1–4. https://doi.org/10.1016/b978-012683630-1/50020-5

[3] Foster, J. L., and Estes, H. S., "A Parametric Analysis of Orbital Debris Collision Probability and Maneuver Rate for Space Vehicles," NASA JSC-25898, Aug. 1992.

[4] Chan, K., *Spacecraft Collision Probability*, Aerospace Corp., El Segundo, CA, 2008, Chaps. 1–8. https://doi.org/10.2514/4.989186

[5] Alfano, S., "Satellite Conjunction Monte Carlo Analysis," *AAS Space Flight Mechanics Meeting*, American Astronautical Soc. Paper 09-233, Feb. 2009.

[6] Sabol, C., Binz, C., Segerman, A., Roe, K., and Schumacher, P. W., Jr., "Probability of Collisions with Special Perturbations Using the Monte Carlo Method," *AIAA/AAS Astrodynamics Specialist Conference*, AIAA Paper 2011-435, Aug. 2011.

[7] Schilling, B., Talib, Y., Carpenter, J. R., Balducci, M., and Williams, T. W., "Operational Experience with the Wald Sequential Probability Ratio Test for Conjunction Assessment from the Magnetospheric Multi-Scale Mission," *AIAA/AAS Astrodynamics Specialist Conference*, AIAA Paper 2016-5424, Sept. 2016. https://doi.org/10.2514/6.2016-5424

[8] Hall, D. T., Casali, S. J., Johnson, L. C., Skrehart, B. B., and Baars, L. G., "High-Fidelity Collision Probabilities Estimated Using Brute Force Monte Carlo Simulations," *AAS Astrodynamics Specialist Conference*, American Astronautical Soc. Paper 18-244, Aug. 2018.

[9] Vallado, D. A., *Fundamentals of Astrodynamics and Applications*, 2nd ed., Microcosm Press, El Segundo CA, 2001.

[10] Akella, M. R., and Alfriend, K. T., "The Probability of Collision Between Space Objects," *Journal of Guidance, Control, and Dynamics*, Vol. 23, No. 5, 2000, pp. 769–772. https://doi.org/10.2514/2.4611

[11] Hall, D. T., "Implementation Recommendations and Usage Boundaries for the Two-Dimensional Probability of Collision Calculation," *AAS Astrodynamics Specialist Conference*, American Astronautical Soc. Paper 19-632, Aug. 2019.

[12] Patera, R. P., "Collision Probability for Larger Bodies Having Nonlinear Relative Motion," *Journal of Guidance, Control, and Dynamics*, Vol. 26, No. 5, 2003, pp. 728–733. https://doi.org/10.2514/1.23509

[13] Coppola, V. T., "Including Velocity Uncertainty in the Probability of Collision Between Space Objects," *AAS/AIAA Spaceflight Mechanics Meeting*, American Astronautical Soc. Paper 12-247, Feb. 2012.

[14] DeMars, K. J., Cheng, Y., and Jah, M. K., "Collision Probability with Gaussian Mixture Orbit Uncertainty," *Journal of Guidance, Control, and Dynamics*, Vol. 37, No. 3, 2014, pp. 979–985. https://doi.org/10.2514/1.62308

[15] Jones, B. A., and Doostan, A., "Satellite Collision Probability Estimation Using Polynomial Chaos Expansions," *Advances in Space Research*, Vol. 52, No. 11, 2013, pp. 1860–1875. https://doi.org/10.1016/j.asr.2013.08.027

[16] Chan, K., "Formulation of Collision Probability with Time-Dependent Probability Distribution Functions," *AAS/AIAA Space Flight Mechanics Meeting*, American Astronautical Soc. Paper 15-233, Jan. 2015.

[17] Chan, K., "Hovering Collision Probability," *AAS/AIAA Space Flight Mechanics Meeting*, American Astronautical Soc. Paper 15-234, Jan. 2015.

[18] Shelton, C. T., and Junkins, J. L., "Probability of Collision Between Space Objects Including Model Uncertainty," *Acta Astronautica*, Vol. 155, 2019, pp. 462–471. https://doi.org/10.1016/j.actaastro.2018.11.051

[19] Mashiku, A. K., and Hejduk, M. D., "Recommended Methods for Setting Mission Conjunction Analysis Hard Body Radii," *AAS Astrodynamics Specialist Conference*, American Astronautical Soc. Paper 19-702, Aug. 2019.

[20] Hall, D. T., Hejduk, M. D., and Johnson, L. C., "Time Dependence of Collision Probabilities During Satellite Conjunctions," *AAS Space-Flight Mechanics Meeting*, American Astronautical Soc. Paper 17-271, Feb. 2017.

[21] Anon., "Conjunction Data Message," Recommended Standard, Consultative Committee for Space Data System, CCSDS 508.0-B-1, June 2013 with addendum Cor. 1, June 2018, https://public.ccsds.org/Pubs [retrieved 01 Jan. 2020].

[22] Hall, D. T., and Matney, M. J., "Collision Probabilities for Keplerian Orbits," *Space Debris*, Vol. 2, 2000, pp. 161–198.

[23] Broucke, D. T., and Cefola, P. J., "On the Equinoctial Orbit Elements," *Celestial Mechanics*, Vol. 5, No. 3, 1972, pp. 303–310. https://doi.org/10.1007/bf01228432

[24] Sabol, C., Sukut, T., Hill, K., Alfriend, K., Write, B., Li, Y., and Schumacher, P., "Linearized Orbit Covariance Generation and Propagation Analysis via Simple Monte Carlo Simulations," *AAS/AIAA Space Flight Mechanics Meeting*, American Astronautical Soc. Paper 10-134, Feb. 2010.

[25] Papoulis, A., *Probability, Random Variables, and Stochastic Processes*, 3rd ed., McGraw–Hill, New York, NY, 1991.

[26] Anon., "Astrodynamic Standards Software," U.S. Air Force Space Command, 2018, http://www.afspc.af.mil [retrieved 15 Jan. 2019].

[27] Nielson, P. D., and Alfriend, K. T., "Continuing Kepler's Quest Assessing Air Force Space Command's Astrodynamics Standards," National Research Council of the National Academies, National Academies Press, 2012. https://doi.org/10.17226/13456

[28] Bowman, B. R., Tobiska, W. K., Marcos, F. A., Huang, C. W., Lin, C. S., and Burke, W. J., "A New Empirical Thermospheric Density Model JB2008 Using New Solar and Geomagnetic Indices," *AIAA/AAS Astrodynamics Specialist Conference*, AIAA Paper 2008-6348, Aug. 2008. https://doi.org/10.2514/6.2008-6438

[29] Casali, S. J., and Barker, W. N., "Dynamic Calibration Atmosphere (DCA) for the High Accuracy Satellite Drag Model (HASDM)," *AIAA/AAS Astrodynamics Specialist Conference*, AIAA Paper 2002-4888, Aug. 2002. https://doi.org/10.2514/6.2002-4888

[30] Vallado, D., "Covariance Transformations for Satellite Flight Dynamics Operations," *AAS/AIAA Astrodynamics Specialist Conference*, American Astronautical Soc. Paper 03-526, Aug. 2003.

[31] Vallado, D., and Alfano, S., "Updated Analytical Partials for Covariance Transformations and Optimization," *AAS/AIAA Space Flight Mechanics Meeting*, American Astronautical Soc. Paper 15-537, 2015.

[32] Dirac, P. A. M., *The Principals of Quantum Mechanics*, 4th ed., Oxford Univ. Press, Cambridge, MA, 1958, Chap. 3.

[33] Arfken, G. B., Weber, H. J., and Harris, F. E., *Mathematical Methods for Physicists*, 7th ed., Academic Press/Elsevier, Waltham, MA, 2013, Chaps. 1, 2, 3, and 23. https://doi.org/10.1016/c2009-0-30629-7

[34] Baars, L., Hall, D., and Casali, S., "Assessing GEO and LEO Repeating Conjunctions Using High Fidelity Brute Force Monte Carlo Simulations," *AAS Astrodynamics Specialist Conference*, American Astronautical Soc. Paper 19-612, Aug. 2019.

[35] Clopper, C., and Pearson, E. S., "The Use of Confidence or Fiducial Limits Illustrated in the Case of the Binomial," *Biometrika*, Vol. 26, No. 4, Dec. 1934, pp. 404–413. https://doi.org/10.1093/biomet/26.4.404

[36] Johnson, N. L., Kotz, S., and Kemp, A. W., *Univariate Discrete Distributions*, Wiley, Hoboken, NJ, 1993. https://doi.org/10.1002/0471715816

[37] Carpenter, J. R., "Non-Parametric Collision Probability for Low-Velocity Encounters," *AAS/AIAA Spaceflight Mechanics Meeting*, American Astronautical Soc. Paper 07-201, Jan. 2007.

[38] Horwood, J. T., Aragon, N. D., and Poore, A. B., "Gaussian Sum Filters for Space Surveillance: Theory and Simulations," *Journal of Guidance, Control, and Dynamics*, Vol. 34, No. 6, 2011, pp. 1839–1851. https://doi.org/10.2514/1.53793

[39] Casali, S., Hall, D., Snow, D., Hejduk, M., Johnson, L., Skrehart, B., and Baars, L., "Effect of Cross-Correlation of Orbital Error on Probability of Collision Determination," *AAS Astrodynamics Specialist Conference*, American Astronautical Soc. Paper 18-272, Aug. 2018.

[40] Duncan, M., and Long, A., "Realistic Covariance Prediction for the Earth Science Constellation," *AIAA/AAS Astrodynamics Specialist Conference*, AIAA Paper 2006-6293, Aug. 2006. https://doi.org/10.2514/6.2006-6293

[41] Zaidi, W. H., and Hejduk, M. H., "Earth Observing System Covariance Realism," *AIAA/AAS Astrodynamics Specialist Conference*, AIAA Paper 2016-5628, Sept. 2016. https://doi.org/10.2514/6.2016-5628

[42] Coppola, V. T., "Evaluating the Short Encounter Assumption of the Probability of Collision Formula," *AAS/AIAA Spaceflight Mechanics Meeting*, American Astronautical Soc. Paper 12-248, Feb. 2012.

[43] Petersen, K. B., and Pedersen, M. S., *The Matrix Cookbook*, Technical Univ. of Denmark, Nov. 2012, https://www2.imm.dtu.dk/pubdb/edoc [retrieved 25 Jan. 2020].

[44] Lebedev, V., and Laikov, D., "A Quadrature Formula for the Sphere of the 131st Algebraic Order of Accuracy," *Doklady Mathematics*, Vol. 59, No. 3, 1999, pp. 477–481.

I. I. Hussein
Associate Editor